17618-H076-R0-00

PROJECT TECHNICAL REPORT
TASK E&DD-701A

RADIATIVE, ABLATIVE, AND ACTIVE COOLING THERMAL PROTECTION STUDIES FOR THE LEADING EDGE OF A FIXED-STRAIGHT WING SPACE SHUTTLE, PART I: ANALYTICAL METHODS

NAS 9-8166

31 DECEMBER 1970

Prepared for
NATIONAL AERONAUTICS AND SPACE ADMINISTRATION
MANNED SPACECRAFT CENTER
HOUSTON, TEXAS

Prepared by
A. V. Gomez

Approved by D. C. Gardner
D. C. Gardner, Task Manager

Approved by R. G. Payne
R. G. Payne, Manager
Thermodynamics Department
Aeromechanics Laboratory

TRW
SYSTEMS GROUP

FOREWORD

This report was prepared by TRW Systems Group, Houston Texas, under NASA Manned Spacecraft Contract NAS 9-8166. The report is published in six parts:

Part I : Analytical Methods (Theory)

Part II : Aerodynamic Heating Predictions

Part III: Radiative and Ablative Heat Shields Performance

Part IV : Regenerative Cooled Heats Shields Performance

Part V : Transpiration Cooled Heat Shields Performance

Part VI : Summary Report and Conclusions

The sponsor of the present investigation was the Thermal Protection Section, Structures and Mechanics Division, Manned Spacecraft Center, National Aeronautics and Space Administration, Houston Texas. Miss Emily W. Stephens and Dr. Donald M. Curry were the NASA/MSC technical monitors.

The TRW principal investigator was Mr. Antulio V. Gomez. While a number of people contributed directly or indirectly to the program, the major contributions were made by the following engineers:

Analytical procedures (theory): A. V. Gomez

Performance Calculation & Tradeoff Studies: C. G. Johnston

The authors wish to thank Mrs. Juanice O'Connor and Mrs. Pat Powell of TRW who assisted in the final preparation of the reports.

ABSTRACT

Space shuttle orbiter vehicle concepts adopting a fixed-straight wing configuration present the thermal protection system designer with a critical design problem - protection of the leading edge of the wing during the atmospheric entry flight phase. A number of techniques to adequately protect the leading edge are feasible within current technology. The purpose of the present study is to predict the thermal performance of a number of leading edge thermal protection system concepts and compare the resulting system weights for a range of entry aerothermodynamic environment conditions. Completion of this work will provide MSC management with decision making data necessary for more detailed vehicle design phases. MSC established design goals of low cost, high reliability, light weight, and fully re-usable vehicles requires the use of sophisticated, recently developed, accurate, numerical analysis design tools to be employed in order to perform meaningful tradeoff studies. The thermal protection systems which are considered include: (i) radiative heat shields, (ii) ablative heat shields, (iii) regenerative cooled heat shields, and (iv) transpiration cooled heat shields. Although ablative heatshields do not rigorously fit the requirement of re-usability, this design concept must be included in order to provide a complete picture of the overall advantages and disadvantages of the principal candidate thermal protection systems for the space shuttle application.

TABLE OF CONTENTS

LIST OF FIGURES

LIST OF TABLES

NOMENCLATURE

a_H, a_M boundary layer correlation function weighting constants, defined by:

$$G = \frac{a_H B_H}{EXP(a_H B_\mu) - 1}$$

where

$a = a_H$ for heat transfer

$a = a_M$ for mass transfer

a, b width and depth of a rectangular shaped orifice or passage (regenerative cooling analysis, see figure 5, p.27)

B_H boundary layer blowing parameter for heat transfer defined by:

$$B_H = \frac{\dot{m}}{\rho_e u_e St_H^*}$$

B_{M_i} boundary layer blowing parameter for mass transfer of ith species defined by:

$$B_{M_i} = \frac{\dot{m}}{g_{M_i}} = \frac{c_{i,e} - c_{i,s}}{c_{i,s} - c_{i,t}}$$

B_g' boundary layer blowing parameter for gas species originating from in-depth decomposition of the heat shield material or mechanically injected through a porous wall (equation 3.24, p.24)

B_c' boundary layer blowing parameter for wall or char species (equation 3.28, p.25)

B^* transpiration cooling injectant heat blocking similarity parameter (equation 5.22, p.46)

c species mass fraction (e.g.: c_1, c_j, c_k, etc)

c_p specific heat at constant pressure

$c_{p_{i,mono}}$ specific heat at constant pressure for a monatomic or equivalent monatomic gas-phase species given by:

$$c_{p_{i,mono}} = \frac{4.9681}{M_i} \quad \left(BTU/LBM\text{-}^\circ R\right)$$

c_v specific heat at constant volume

C_f skin friction dimensionless coefficient defined by:

$$C_f = \frac{\tau_w}{\frac{1}{2}\rho V^2}$$

C_n constants, C_1, C_2, C_3, ... C_n

d diameter

NOMENCLATURE (Cont.)

$\bar{d}$ mean pore diameter of porous matrix (equation 5.08, p.36)

D effective diameter of a generalized cylindrical shaped pipe (equation 4.22, p.30)

$\bar{\mathcal{D}}$ reference species mass self diffusion coefficient (equation 6.05, p.59)

$\mathcal{D}_{i,j}$ multicomponent binary mass diffusion coefficient for species i into j

E_T, E_p transpiration cooled matrix property groupings (equation 5.11, p.37)

$F(\frac{F}{\ell})$ heating factor (equation 2.15, p.15)

F_i diffusion factor for the ith species used in determining the multicomponent binary mass diffusion coefficients according to the bifurcation approximation (equation 6.05, p.59)

$F(\ )$ function of ( )

F_m polynomial curve fit coefficients used in determining species thermodynamic properties (equations 6.01 through 6.04, p.58)

g gravitational constant (g = 32.17 ft/sec^2)

G_H boundary layer conduction heat transfer rate to the wall with mass injection normalized by its corresponding value for the limit of zero mass injection (equation 2.04, p.12)

G_M boundary layer mass transfer conductance at the wall for the ith species with mass injection normalized by its corresponding value for the limit of zero mass injection (equation 2.09, p.13)

h static enthalpy

H stagnation enthalpy

H_r recovery enthalpy at the wall

h_f film heat transfer coefficient defined by

$$h_f := \frac{\dot{q}}{h_w - h_b}$$

J constant, J = 778 foot-lbf/Btu

$\dot{J}_i$ mass diffusion flux of ith species

K thermal conductivity

NOMENCLATURE (Cont.)

ℓ reference length

Le_i Lewis Number, $Le_i = \frac{\mathcal{D}_{i,air}}{\alpha_T}$ (equation 2.13, p.14)

M Mach Number

$\mathcal{M}_i$ molecular weight of ith species

$\dot{m}$ mass flux per unit area (lbm/sec-ft^2)

$\dot{\mathcal{M}}$ mass flux per unit width (lbm/sec-ft)

$\dot{m}^*$ transpiration cooling porous matrix dimensionless mass flux (equation 5.11, p.37)

N_u Nusselt Number, $Nu = S_{T_H} Pr \; Re$

p pressure

p^* transpiration cooling porous matrix dimensionless pressure drop (equation 5.11, p.37)

P porous matrix porosity based on the ratio of open to total crosssectional area (equation 5.08, p.36)

P^V porous matrix porosity based on volume (equation 5.09, p.36)

P_r Prandtl Number, $Pr = \frac{c_p \mu}{K}$

$\dot{q}$ heat transfer rate per unit area (Btu/sec-ft^2)

$\dot{q}_{BL}$ boundary layer convective heat transfer rate to the wall (equation 1.03, p.10)

$\dot{q}_F$ regenerative cooling heat transfer rate to the coolant bulk flow (equation 4.01, p.26)

$\dot{q}_{HS}$ conduction heat transfer rate into the heatshield evaluated at the U surface (equation 1.01, p.8)

$\dot{q}_R$ outer flow radiation heat transfer rate to the wall

$\dot{q}_{RR}$ wall surface reradiation heat transfer rate $(\dot{q}_{RR} = \varepsilon \sigma T_w^4)$

$\dot{q}_{REF}$ reference heat transfer rate defined as the stagnation point heat transfer rate to a one foot radius sphere (equation 2.16, p.15)

Q_{ABL} heat of ablation (Btu/lbm)

$Q_{oxid.}$ heat of oxidation due to chemical reactions at the wall interface (equation 1.07 , p.10)

NOMENCLATURE (Cont.)

Q_{SUBL} heat of sublimation due to chemical reactions at the wall interface (equation 1.08, p.10)

Q^* transpiration cooling porous matrix Nusselt Number similarity parameter (equation 5.22, p.46)

r recovery factor

$\vec{r}$ spatial location vector

R universal gas constant (R = 1.98726 g-cal/gram-mole ^{o}K)

R_e Reynolds Number (equation 4.21, p.29)

R_H chemical enthalpy recovery factor (equation 2.01, p.12)
R_H = 1 for inert injectants - no chemical reactions between injectant species and air species.

S outer surface defined in the interface energy balance for the wall (figure 3, p.9)

$\dot{s}$ wall surface recession rate, $\dot{s} = \frac{\dot{m}_c}{\rho_c}$

St_H heat transfer Stanton number, defined by:

$$St_H = \frac{\dot{q}_w}{\rho_e u_e (H_r - h_w)}$$

$St_{M,i}$ mass transfer Stanton Number for the ith species, defined by:

$$St_{M,i} = \frac{\dot{m}_{i,w}}{\rho_e u_e (C_{i,e} - C_{i,w})}$$

St_M^{**} mass transfer Stanton Number definition used in the open surface, chemical state, thermochemistry calculation (equation 3.25, p.25)

t time (seconds)

T temperature

$T^{\hat{*}}$ Eckert reference temperature used in determining variable properties solutions (equation 4.18, p.29)

U inner surface defined in the interface energy balance for the wall (figure 3, p.9)

u velocity component parallel to the wall (parallel to X)

v velocity component normal to the wall (parallel to Y)

V bulk flow velocity

x_i mole fraction of ith. species

NOMENCLATURE (Cont.)

X curvilinear coordinate defined in the streamwise direction of the outer flow (i.e.: boundary layer flow) and parallel to the wall (figures 5 and 6, pp. 27 and 38)

Y curvilinear coordinate normal to the wall surface (figures 5 and 6)

Z^* transpiration cooling porous matrix cooling ratio similarity parameter (equation 5.22, p.46)

α wing angle of attack

α' transpiration cooling dimensionless property grouping $\alpha' = \frac{c_{p_\ell}}{c_{p_g}}$ (equation 5.15a, p.40)

α_T thermal diffusivity, $\alpha_T = \frac{K}{\rho c_p}$

α_I^* transpiration cooling dimensionless inertial resistance coefficient (equation 5.11b, p.37)

Γ_1, Γ_2 porous matrix permeability coefficients (equation 5.01, p.33)

ΔE activation energy (equation 3.07, p.17)

Δh_f heat of formation of ith. species at 298°K

Δh_v heat of vaporization

δX linear step increment in the streamwise direction

ϵ gray body radiation emissivity coefficient

ϵ_p transpiration cooling dimensionless property grouping (equation 5.15e, p.40)

ζ transpiration cooling dimensionless property grouping, $\zeta = \alpha(\theta_p - 1)$ (equation 5.15d, p.40)

θ porous matrix flow dimensionless temperature, $\theta = \frac{T}{T_o}$

μ absolute coefficient of viscosity

ν total number of species considered

ξ_η $(\eta = 1,4)$ transpiration cooled matrix flow dimensionless scaling parameters (equation 5.05, p.34)

π constant, $\pi = 3.14159$

ρ density

ρ_R gray radiation wall surface reflectance coefficient

σ Stefan-Boltzman constant, $= 0.4761 \times 10^{-12}$ Btu/sec-ft^2-$^\circ$R

τ shear stress

$\bar{\tau}$ porous matrix effective one dimensional thickness

$\bar{\Phi}$ viscous dissipation

ϕ porous matrix design pressure ratio $\phi = \frac{p_i}{p_{e(X)}}$

ϕ_v transpiration cooling dimensionless property grouping, $\phi_v = \frac{\Delta h_v}{c_{p_g} T_o}$ (equation 5.15c, p.40)

SUBSCRIPTS:

air air species

b bulk flow

BL boundary layer

c conduction

c wall or char

cw cold wall

$C.P.$ critical injection control point

$Coolant$ coolant species

D diffusion rate limited oxidation

e equilibrium

e outer edge flow

F fluid

g gas

H heat transfer

HS heat shield

i injectant

i inlet

i, j, k molecular species subscript designations

K kinetic rate limited oxidation

SUBSCRIPTS (Cont.)

ℓ	liquid
m	porous matrix
M	mass transfer
$oxid$	oxidation
o	evaluated at reservoir or back face chamber conditions
p	product species
P	evaluated at the liquid-vapor phase change temperature and pressure
r	reference state
ν	reactant species
REF	reference
R	radiation
RR	reradiation
$\tilde{r}$	mechanical removal or erosion
s	evaluated at the S surface (figure 3, p.9)
SL	sea level
$Subl.$	sublimation
t	transferred state (equation 2.08, p.13)
u	evaluated at the U surface (figure 3, p.9)
w	wall
(X)	function of streamwise coordinate X
(X_m)	evaluated at the streamwise coordinate X corresponding to maximum heating rate
ϕ	oxidizer species (oxygen)
∞	free stream conditions

NOMENCLATURE (Cont.)

SUPERSCRIPTS:

s	solid phase species
$\cdot$	time derivative
$*$	evaluated in the limit of zero mass injection
$'$	past calculated values
a	alternate formulation
v	volume based

INTRODUCTION

Space shuttle orbiter vehicle concepts adopting a fixed-straight wing configuration present a critical thermal protection design problem: the protection of the wing leading edge during the atmospheric entry phase. Radiative heat shields and active cooling thermal protection systems have been identified as possible solutions for reusable space shuttle configurations (Figure 1). Ablative heat shields, although simpler solutions, do not fit exactly the reusability criterion due to the need of ablator replacement after one or a limited number of entry missions. It is obvious that reusable vehicles with long life and low refurbishing costs will break even at some number of missions and yield a decisively superior cost advantage beyond that number. Radiative heat shields are limited by the material's radiative, oxidation chemistry and melting temperature which severely restrict the space shuttle entry trajectory. This results in an undesirable limited cross-range capability. Actively cooled heat shields do not place such a limitation on the shuttle design. Under this concept, regenerative cooling and transpiration cooling systems must be considered. In regenerative cooling thermal protection is obtained by forced convection of coolants at the critical areas of the space shuttle. Heat is carried away by the coolant from the hot spots to other areas of the vehicle where it may be dumped, radiated away or soaked in, i.e., heat sink. For transpiration cooling, the coolant is injected into the external flow at the critical surface areas where thermal protection is required. Thermal protection is achieved in two ways; first, by the heat absorbed by the coolant as it flows through the porous wall material which is called a matrix, and second, by considerably altering the external flow near the wall (the boundary layer) in a manner which results in a substantial decrease in the convective heat transfer rate to the wall, the so-called boundary layer heat blocking effect.

Three representative entry trajectories for a 25,000 pound payload space shuttle orbiter with a fixed-straight wing configuration were selected for analysis. During entry the wing angle of attack is held constant at 60°, 45° or 22.5° which provided for a cross range capability of 313, 624 and 1196 nautical miles for each entry trajectory respectively (Figure 2).

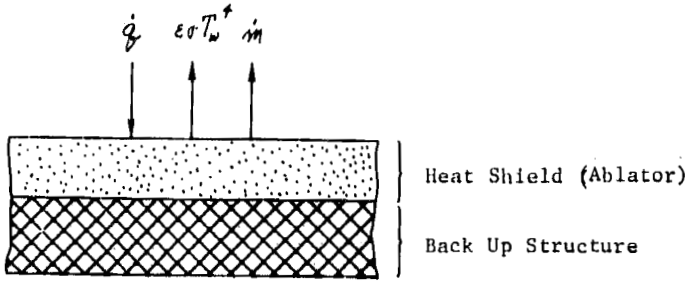

A - Radiative and Ablative Heat Shield

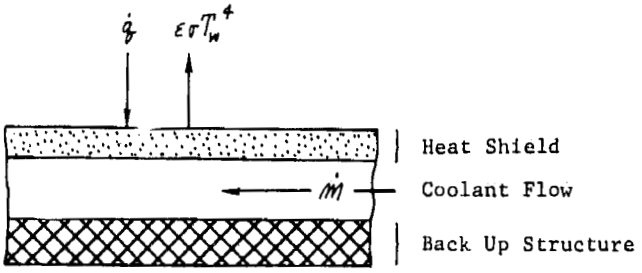

B - Regenerative Cooled Heat Shield

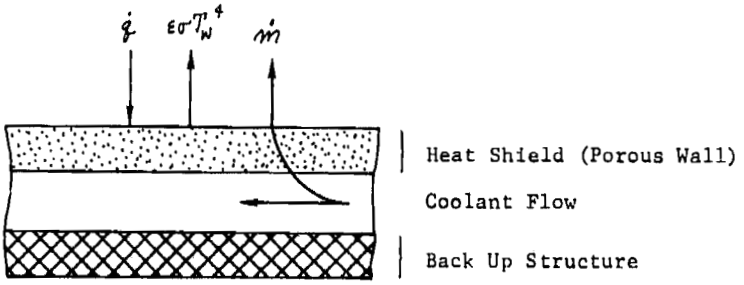

C - Transpiration Cooled Heat Shield

FIGURE 1 - HEAT SHIELD DESIGN OPTIONS

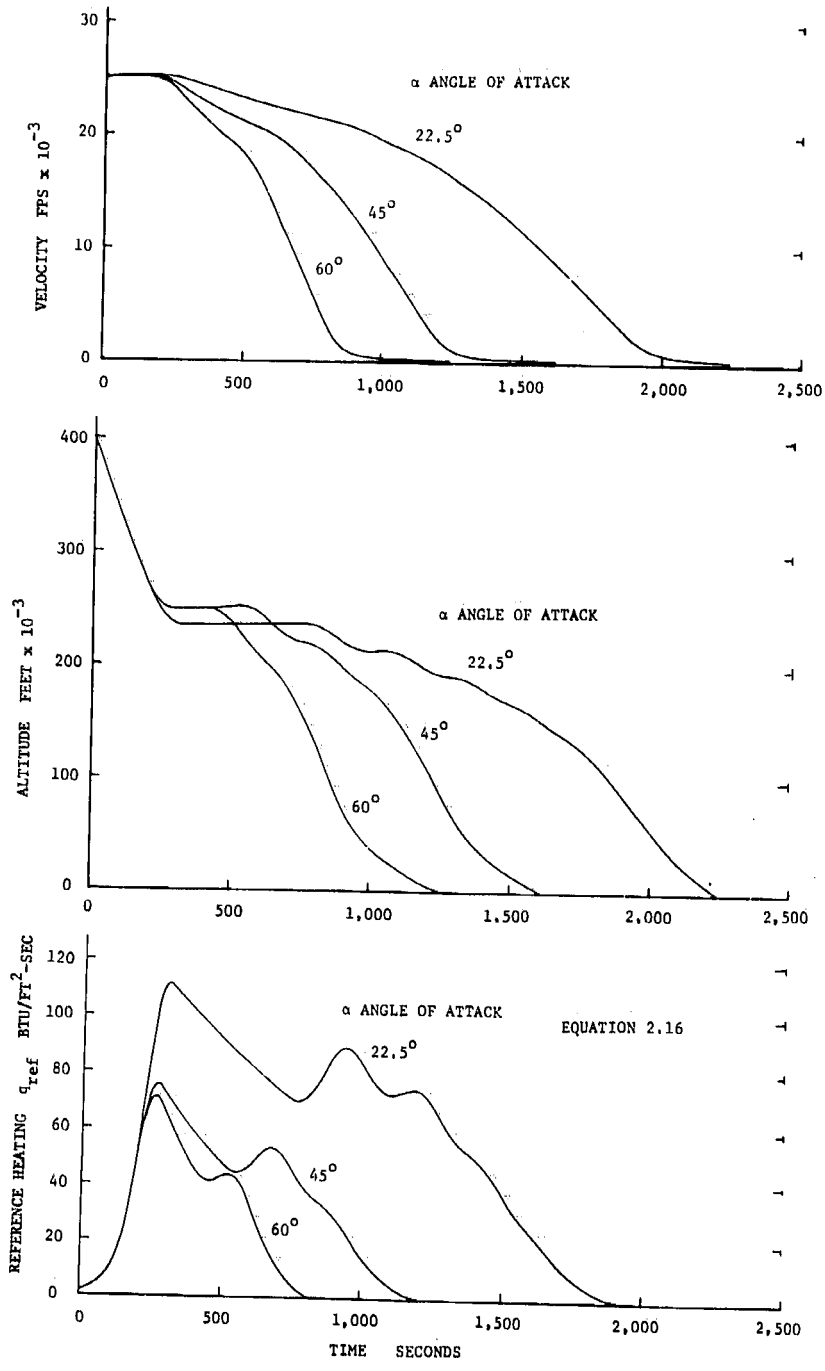

FIGURE 2 - ENTRY TRAJECTORIES

The prescribed wing geometry is presented in Table 1. The determination of the heating environment for each trajectory (the cold wall convective heating) was performed using theoretical and semi-empirical methods. For the theoretical method the flow on the wing was assumed two dimensional (no cross flow) but accounted for the hypersonic viscous interaction effects at the leading edge. The semi-empirical methods were based on comprehensive two-dimensional and three-dimensional wind tunnel tests. This led to the definition of three entry heating environments for each entry trajectory which are designated 2-D theory, 2-D empirical, and 3-D empirical. The peak heating was found to vary as much as a factor of three depending on the method of calculation selected.

TABLE 1 - WING GEOMETRY

Area	1175.0 ft^2
Span	90.43 ft
Exposed Span	70.25 ft
Aspect Ratio	6.96
Taper Ratio	0.353
Leading Edge Sweep Angle	14°
Airfoil Section	NACA 0012-64

The methods for determining the surface degradation or recession for radiative and ablative heatshields were based on arc jet test correlations, when available, and recently developed theory. The theoretical methods properly accounted for the wall surface thermochemistry and the effects on the heat and mass diffusion fluxes at the wall due to the injection of foreign species into the external flow. Theoretical predictions were made for the materials for which arc jet testing data was available and the results obtained were compared and found to be in excellent agreement with the empirical results. The methods of analyzing the various heat shield materials selected varied depending on the melt temperature and oxidation chemistry. Generally they may be categorized as (i) oxidation controlled - when their melting temperature is found to be much greater than the radiative equilibrium temperature for the calculated convective heat transfer rate, (ii) simple sublimers - when the melting temperature is lower than

the radiative equilibrium temperature, and (iii) pyrolytic ablators - where the material decomposition into pyrolysis gas and char occurs in depth. In all cases, the heat of ablation was determined by considering as many species as possible for which thermochemical data was available. The thermodynamic properties of the species were determined from curve fits to JANAF data and other sources.

For regenerative cooling, the wing leading edge was assumed constructed with small orifices or passages where the coolant flows. The flow in these passages was assumed to be either laminar or turbulent depending on the Reynolds number and in the liquid or gaseous phase depending on the inlet conditions. The coolant properties were calculated through curve fits to JANAF thermochemical data. The inlet conditions were determined as a function of the required pressure to achieve the proper flow. The corresponding inlet temperature and density were determined from the coolant temperature-entropy charts by assuming an arbitrary heat addition cycle followed by an isentropic expansion or compression of the coolant. Viscous dissipation (heating) and the wall surface reradiation were included in the analysis. To obtain solutions, the wall (skin) was assumed to be at the equilibrium temperature from which the coolant temperature gradient, pressure gradient and velocity gradients were calculated. The procedure followed for obtaining solutions was based on finite step (differences) numerical analysis and iterations were performed until a satisfactory solution was obtained. The criterion for determining satisfactory solutions depended on the maximum wall temperature desired and on the fact that the flow Mach number cannot exceed one.

Transpiration cooling is provided by gas or liquid injection through a porous wall or matrix of either connected open porosity or a simulation of this by many small discrete holes or capillary tubes distributed over the wall. As a matter of fact, the theory of flow through a porous matrix is based on the analysis of flow through capillary tubes. In this manner a continuous distribution of coolant injection to the exposed surface is achieved which may be varied according to the heating requirements by varying the permeability and the thickness of the matrix. Because of this fact this system features the most efficient utilization of the injectant. Since the coolant injection is distributed over an area, local

flow rates are moderate and the character of the outer flow is not drastically altered. Therefore current single phase multicomponent injection boundary layer theory adequately portrays the outer flow. Comparing this with film cooling, where the injection is achieved through a finite number of discrete size orifices or ports, the coolant must be injected at sufficient rates in order that a thin liquid or vapor film made out of the injectant species is formed between the exposed wall surface and the reentry environment. This film acts as an insulating layer which provides the required thermal protection. In this instance the character of the flow is altered substantially and the usual single phase multicomponent injection boundary layer theory is no longer applicable to the analysis of the problem. Instead, more difficult complete solution procedures for the external flow field must be developed. These must include: two phase flow, strong non-similar blowing effects, and the stability of the film under the high shear environment of reentry. These difficulties dictate that new advancements in the formulation of analytical procedures must be accompanied by extensive experimental test programs.

The advantages of transpiration cooling over other thermal protection systems have been demonstrated in many studies completed in recent years. These studies invariably considered the flow through the porous wall separate from the injection heat blocking effects. Therefore, attention has been directed to the solution of the coupled problem (matrix flow-heat blocking effects) with the objective of determining the overall system performance and injection control requirements. Analytical predictions for the coupled problem show that the characteristic behavior of both gas and liquid coolants exhibit a region of unstable flow where injection control by varying the inlet pressure is ineffective. The matrix temperature and the injectant properties play an important part with respect to the injection control. When the mass injection rates are reduced sufficiently, injection control is lost. In this region, the outer wall boundary conditions and the heat stored in the matrix govern the flow rate regardless of the backface pressure. This condition is akin to ablation where the outer wall conditions govern the mass injection into the boundary layer. This phenomenon is found to be characteristic of gas as well as liquid injection. For liquids, the unstable region is encountered when a vapor phase change is present in the matrix. The

surprising result is that this instability is found for gases as well even though no phase change occurs. The prediction of the onset of the critical region incorporated in the present analysis is of great importance in order to ensure adequate injection control and hence the survival of the porous wall.

In the present report (Part I of 6 parts), the formulation of the analytical models and solution procedures for the preceding thermal protection design concepts(Figure 1,pp.2) for application to representative space shuttle entry missions are considered exclusively.

PART I: ANALYTICAL METHODS (THEORY)

1. Wall Interface Energy Balance

Consider the wall mass and energy flux balance presented in Figure 3. In the figure a small control volume is presented which encloses the wall surface and is bounded by the mathematical surfaces S and U. These surfaces are assumed to lie very close to the wall such that the control volume width is negligibly small in comparison with the characteristic dimensions of the boundary layer, i.e., the boundary layer thickness. At the S surface the wall gas phase properties are defined. Some properties are continuous across the wall, e.g., T and $\dot{m}$, while others are discontinuous, e.g., h and c. In this manner the boundary layer and heat shield mass and energy fluxes may be precisely defined even though chemical reactions are occurring at the physical surface. The relations prescribing conservation of energy and conservation of mass for steady state at the wall interface are:

$$\dot{q}_{HS} = \dot{q}_{c,u} = \left[\dot{q}_c - \sum_{i=1}^{\nu} \dot{m}_i h_i\right]_s + \left[\dot{m}_g h_g + \dot{m}_c h_c^s\right]_u + \dot{q}_R(1-\rho_R) - \varepsilon\sigma T_w^4 \qquad (1.01)$$

$$\dot{m} = \sum_{i=1}^{\nu} \dot{m}_i = \dot{m}_g + \dot{m}_c \qquad (1.02)$$

In this formulation*, mechanical removal of the wall material is neglected and the boundary layer flow is assumed transparent to radiation. The temperatures at the S, U, and wall surface are assumed to be equal (this assumption is consistent with the assertion that the control volume thickness is negligibly small). The temperature is a characteristic thermodynamic quantity uniform within the control volume and is dependent on the heat shield response time-integrated heat input and thermodynamic properties. $\left[\int \dot{q}_{HS}\, dt\right]$

*For notation refer to nomenclature list.

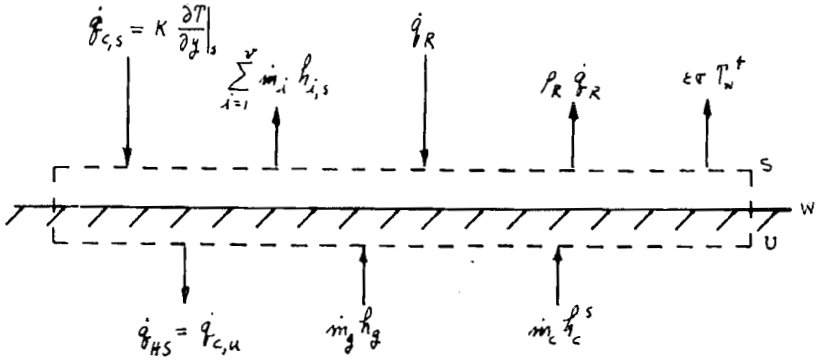

A - Wall mass and energy balance defined in terms of absolute velocity species fluxes

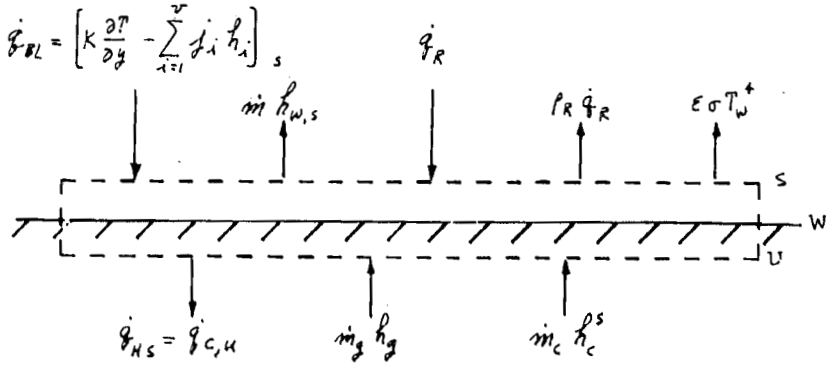

B - Wall mass and energy balance defined in terms of mass average velocity and species diffusion fluxes

FIGURE 3- WALL INTERFACE ENERGY BALANCE

The boundary layer energy fluxes at the S surface relevant to the boundary layer analysis are:

a) the diffusive energy flux to the wall (also called the convective heat transfer rate to the wall)

$$\dot{q}_{BL} = \left[\dot{q}_c - \sum_{i=1}^{v} J_i h_i \right]_s = \left[K \frac{\partial T}{\partial y} - \sum_{i=1}^{v} J_i h_i \right]_s \qquad (1.03)$$

b) the convective energy flux from the wall

$$\dot{m} h_w = \dot{m} h_s = \left[\rho v \sum_{i=1}^{v} c_i h_i \right]_s \qquad (1.04)$$

These definitions result from the treatment of the boundary layer governing equations in terms of mass average velocities. Using absolute species velocities, they are equivalent to:

$$\dot{q}_{BL} - \dot{m} h_w = \left[\dot{q}_c - \sum_{i=1}^{v} \dot{m}_i h_i \right]_s \qquad (1.05)$$

The conduction heat flux rate into the heat shield evaluated at the U surface given by equation 1.01 can be written as:

$$\dot{q}_{HS} = \dot{q}_{c,s} + \dot{m} Q_{OXID} - \dot{m}_c Q_{SUBL} + \dot{q}_R (1 - \rho_R) - \varepsilon \sigma T_w^4 \qquad (1.06)$$

The wall heat of oxidation and heat of sublimation due to chemical reactions which occur within the control volume are obtained from the preceding relations. They are given by:

$$Q_{OXID} = \frac{1}{\dot{m}} \left\{ \left[\dot{m}_g h_g + \dot{m}_c h_c \right]_u - \left[\sum_{i=1}^{v} \dot{m}_i h_i \right]_s \right\} \qquad (1.07)$$

$$Q_{SUBL} = \left[h_c - h_c^s \right]_u \qquad (1.08)$$

$$(Q_{ABLATION} = Q_{OXID} + Q_{SUBL})$$

where h_c^s is the solid phase enthalpy of the wall species.

2. Boundary Layer Heat and Mass Transfer Fluxes at the Wall

The most refined method for predicting the boundary layer heat and mass transfer fluxes to the wall which is presently available involves the coupling of a numerical solution procedure for the boundary layer flow conservation equations to a finite difference solution procedure for the in-depth response of the heatshield. Such an approach is not feasible for performing engineering calculations over a complete entry trajectory; this is due to the excessive computer time required and the inherent unreliability of such a complex computer program. Thus current practice involves a finite difference solution of the conservation equations governing the in-depth response of the heat shield, but uses simple correlation formulae to describe the convective heat and mass transfer fluxes to the wall. These formulae are in the form of standard correlations for high temperature boundary layer flows with correction factors to account for the reduction of heat and mass transfer due to surface mass addition. For example, the formula of Hoshizaki[1]* might be used to predict the stagnation point heat transfer, and this value corrected for the effect of mass addition in the manner recommended by Lees.[2] The most extensive computations of these "blockage factors" are those of Gomez et al[3] and Mills et al[4], which include multicomponent diffusion effects and chemical reactions between injectant and air species. These correlations are of rather general validity but, in particular, are applicable to the aerothermochemical environment characteristic of reentry from lunar missions. The correlations are of the exponential form suggested by a Couette flow model, with empirical parameters adjusted so as to yield a best fit of data for injectant species molecular weights ranging from diatomic hydrogen ($M = 2.016$) to Xenon ($M = 131.3$).

*Superscript numbers denote references listed on p. 60.

The Gomez-Mills correlations are:

Heat Transfer

$$\dot{q}_{HS} = \dot{q}_{c,u} = \dot{q}_{c,u}^{\,I} R_f + \dot{q}_R (1 - \rho_R) - \varepsilon \sigma T_w^4 \qquad (2.01)$$

$$\dot{q}_{c,u}^{\,I} = \left[\dot{q}_c - \sum_{i=1}^{v} \dot{m}_i h_i \right]_s^I + \left[\dot{m}_g h_g + \dot{m}_c h_c^s \right]_u \qquad (2.02)$$

$$\dot{q}_{c,s}^{\,I} = \dot{q}_{c,s}^{\,*} \; G_H \qquad (2.03)^*$$

$$G_H = \prod_{i=1}^{v} \frac{a_{H_i} \, c_{i,t} \, B_H}{EXP \; a_{H_i} \, c_{i,t} \, B_H \; - 1} \qquad (2.04)$$

$$\phi_i = 1.25 \left\{ \left(\frac{M_{air}}{M_i} \right)^{0.4} \left(\frac{c_{p_i}}{c_{p_i, mono}} \right)^{0.3} \right\} \qquad (2.05)$$

$$B_H = \frac{\dot{m}}{\rho_e u_e S T_H^*} = \frac{\dot{m}}{\left(\dfrac{\dot{q}_{c,s}^{\,*}}{\left[H_r - h_{w(T_w)} \right]_{air}} \right)} \qquad (2.06)^*$$

$$\dot{q}_{c,s}^{\,*} = \dot{q}_{cw(T_{REF})} \left[\frac{H_r - h_w(T_w)}{H_r - h_w(T_{REF})} \right]_{air} \qquad (2.07)^*$$

*Starred quantities are evaluated in the limit of zero mass injection ($B_H \to 0$).

Mass Transfer*

$$\dot{m}_i = \dot{m}\, c_{i,s} + j_{i,s} = \dot{m}\, c_{i,t} \tag{2.08}$$

$$g_{M_i} = g_{M_i}^{*}\, G_{M_i} = \frac{-j_{i,s}}{c_{i,e} - c_{i,s}} \tag{2.09}$$

$$G_{M_i} = \frac{a_M B_H}{EXP(a_M B_H) - 1} \tag{2.10}$$

$$a_M = 1.125 \left[\mathcal{M}_{air} \sum_{i=1}^{\nu} \frac{c_{i,t}}{\mathcal{M}_i} \right]^{2/3} \tag{2.11}$$

$$g_{M_i}^{*} = \rho_e u_e St_H^{*} Le_i^{0.72} \tag{2.12}$$

The quantity $\dot{q}_{c,u}^{I}$ introduced in equation 2.01, is the effective conduction heat flux into the heat shield evaluated at the U surface in the absence of chemical reactions between injectant and air species in the boundary layer flow and negligible radiation fluxes at the wall. The factor R_h, which is called the chemical enthalpy recovery factor, scales the effect on the conduction heat flux to the heat shield due to these chemical reactions. $R_h = 1$, implies inert injectant species in the boundary layer but it does not exclude the presence of chemical reactions at the wall interface. The quantities g_{M_i}, and $c_{i,t}$ introduced in equations 2.08 and 2.09 are the usual definition of mass transfer conductance and transfer state mass fraction for the ith species which are derived in the Spalding[5] formulation of the steady state mass transfer problem.

*A more accurate but more complex correlation is given by Gomez[14]

$$G_{M_i} = \frac{g_{M_i}}{g_{M_i}^{*}} = \frac{a_{M_i}^{m} B_{M_i}}{EXP(a_{M_i}^{m} B_{M_i}) - 1} \tag{2.10a}$$

$$a_{M_i}^{m} = \left(\sum_{i=1}^{\nu} c_{i,t}\, a_{M_i} \right) \left(\frac{a_{M_i}}{\sum_{i=1}^{\nu} c_{i,t}\, a_{M_i}} \right)^{1/3} \tag{2.11a}$$

where

$$B_{M_i} = \frac{\dot{m}}{g_{M_i}^{*}} \quad , \quad a_{M_i} = 1.462 \left(\frac{\mathcal{M}_{air}}{\mathcal{M}_i} \right)^{0.922}$$

The correlation of mass transfer and heat transfer conductances in the limit of zero mass injection (equation 2.12) introduces the effective binary Lewis Number which is defined by

$$Le_i = \left(\frac{\alpha_T}{\mathcal{D}_{i,air}} \right)^{-1} \quad \text{(the Lewis number)} \qquad (2.13)$$

where

α_T = the frozen thermal diffusivity of the air species evaluated at the wall boundary conditions

$\mathcal{D}_{i,air}$ = the effective binary diffusion coefficient of the ith species into air species

According to the bifurcation approximation of binary diffusion coefficients[6], $D_{i,air}$ may be evaluated using

$$\mathcal{D}_{i,air} = \frac{\bar{\mathcal{D}}_{REF}}{\left(\frac{\mathcal{M}_i}{32}\right)^{0.461} \left(\frac{\mathcal{M}_{air}}{32}\right)^{0.461}} \qquad (2.14)$$

where

$\bar{\mathcal{D}}_{REF}$ = the binary self diffusion coefficient for molecular oxygen ($\mathcal{M}$ = 32) at wall temperature and pressure

$\mathcal{M}_i$ = the ith species molecular weight

$\mathcal{M}_{air}$ = the air mixture mean molecular weight evaluated at the S surface

The cold wall heating rate q_{cw} is determined using either wind tunnel tests of the wing and the complete space shuttle configuration or using current aerodynamic heating 2-dimensional flow theory. The empirical criterion is based on the definition of heating factors which are assumed invariant with entry time. These factors are the ratios of the wind tunnel heating rates, corrected for cold wall effects,

i.e., T_{ref} and scaled to the full size vehicle, normalized by the heating rate to a one-foot radius sphere at the same heating environment. Accordingly, using the Detra, Kemp, and Riddell[7] correlation:

(Empirical)

$$\dot{q}_{CW}(T_{REF}) = \dot{q}_{REF} \; F\left(\frac{\vec{r}}{\ell}\right) \tag{2.15}$$

$$\dot{q}_{REF} = \frac{17{,}600}{\sqrt{1\,FT}} \sqrt{\frac{\rho_\infty}{\rho_{SL}}} \left(\frac{V_\infty}{26{,}000\ FPS}\right)^{3.15} \left(\frac{H_r - h_w(T_{REF})}{H_r - h_w(300°K)}\right)_{air} \left(\frac{BTU}{FT^2 - SEC}\right) \tag{2.16}$$

The theory employed in determining the cold wall heating rate is based on the assumption of two dimensional flow over the exposed wing span. Thus the cross flow effects, which are largest at the highest angle of attack entry trajectory (α = 60°), and the fuselage bow shock impingement on the wing are neglected. To determine the cold wall heating rate, the inviscid shock layer flow field ahead of the wing was investigated using a hypersonic blunt body analysis program.[8] The shock layer solution provides the appropriate pressure and entropy outer edge boundary conditions for the boundary layer calculations from which the cold wall heating rates are obtained. Exact numerical solutions for laminar flow[9] and approximate laminar and turbulent solutions[10] for the boundary layer can then be obtained.

3. Radiative and Ablative Heat Shields

Five separate analytical procedures for determining the heat shield performance which are applicable to the range of materials selected are considered: (i) radiative heatshield, (ii) simple sublimer, (iii) reaction rate limited oxidation, (iv) diffusion limited oxidation, (v) transition regime and (vi) complex ablators, e.g.: pyrolytic heat shield ablators.

3.1 Radiative Heat Shield

In the absence of ablation ($T_{wall} \ll T_{melt}$), the wall temperature has been determined to correspond closely with the equilibrium radiation temperature, T_e, for a wide range of heat shield materials of finite thicknesses (~ 0.15 inches).[11] Neglecting the wall incident radiation, which is negligibly small in comparison with the boundary layer convective heat transfer rate, the wall interface energy balance yields:

$$\dot{q}_{cw(T_{REF})} \left(\frac{H_r - h_w(T_e)}{H_r - h_{w(T_{REF})}} \right)_{air} = \varepsilon \sigma T_e^4 \qquad (3.01)$$

$$\left[h_{w(T_e)} \doteq \left(h_{w(T_{REF})} + c_{p(T_{REF})} \left(T_e - T_{REF} \right) \right)_{air} \right]$$

T_e can be readily solved for by the method of successive approximations.

3.2 Simple Sublimer

In the presence of ablation, the heat of oxidation, the heat of sublimation, and the boundary layer heat blocking effects due to mass injection must be included in the wall interface energy balance. For a simple sublimer, the wall temperature is assumed constant and equal to the melting temperature of the heat shield material ($T_w = T_{MELT}$). If the change of phase (e.g.: $C^s \rightarrow C^g$) of the wall material is the only chemical reaction considered:

$$Q_{SUBL} = \left[h_c - h_c^s \right]_w \qquad (3.02)$$

$$\left[Q_{OXID} = 0 \quad , \quad R_h = 1.0 \right]$$

The wall interface energy balance (equations 1.06, 2.01 through 2.07) yields:

$$\dot{q}_{HS} = \dot{q}_{c,s}^{*} \left[\frac{a_H B_H}{EXP(a_H B_H) - 1} \right] - \dot{m}_c Q_{SUBL} + q_R (1 - \rho_R) - \varepsilon \sigma T_w^4$$

$$(\dot{m} = \dot{m}_c \quad , \quad c_{j,t} = 1.0) \qquad (3.03)$$

where

$$\dot{q}^{*}_{c,s} = \dot{q}_{cw(T_{REF})} \left(\frac{H_r - h_{w(T_w)}}{H_r - h_{w(T_{REF})}} \right)_{air} \qquad (3.04)$$

Neglecting the heat capacitance of the heat shield material and the incident radiation ($q_{HS} \equiv q_R \equiv 0$), equation 3.03 yields:

$$\frac{a_H \; B_H}{EXP(a_H \; B_H) - 1} = B_H \frac{Q_{SUBL}}{\left[H_r - h_{w(T_w)}\right]_{air}} + \frac{\varepsilon \sigma T_w^4}{q^{*}_{c,s}} \qquad (3.05)$$

The blowing parameter B_H can be solved for by the method of successive approximations. The surface degradation rate is obtained using

$$\dot{s} = \frac{\dot{m}_c}{\rho_c} = B_H \; \frac{\dot{q}^{*}_{c,s}}{\left(H_r - h_{w(T_w)}\right)_{air}} \; \frac{1}{\rho_c} \qquad (3.06)$$

The mass transfer correlations provide the information required to determine the heat blocking weighting constant a_H. For the simple sublimer, the trivial solution for the transferred state mass fractions of $c_{i,t} = 1.0$ for the single injectant species and $c_{i,t} = 0$ for the air species applies. Then, using equation 2.05, a_H may be evaluated.

3.3 Reaction Rate Limited Oxidation

It has been shown that all metal-oxygen reactions are first order complex chain reactions[12] whose rate of attack to the metal surface is described by

$$\dot{m}_K = \dot{m}_c = k_1 \left(p_{O_2}\right)^{n} EXP\left(-\frac{\Delta E}{R T}\right) \qquad (3.07)$$

where k_1 is a constant, p_{O_2} is the pressure of oxygen at the metal surface, ΔE is the activation energy (g-cal/gram-mole), R is the universal gas constant (1.98726 g-cal/gram-mole°K) and T is the wall temperature in degrees Kelvin. Since the exponent n lies between zero and unity, linear kinetics are implied.

Finite difference numerical solutions for the heat shield response using equation 3.07 are readily obtainable. For example, at a given entry trajectory time, the wall temperature which is a function of the time-integrated conduction heatflux into the heat shield $\left[\int q_{HS} \, dt \right]$ is determined from the previous time heat-shield in-depth response solution. Then, the ablation rate $\dot{m}$ can be determined. The conduction heat flux into the heat shield at the selected time can next be calculated using the wall interface energy balance and the aerodynamic heating relations (e.g.: equations 1.01 through 2.16 which are exact, or equation 3.03). For application to the present space shuttle, the wall temperature history determined from exact analysis (which includes the heat shield in-depth response) has been found to closely correspond with the equilibrium radiation temperatures. Therefore as a first order approximation, the equilibrium radiation temperature may be used to determine the ablation mass loss rate (equation 3.01 and 3.07).

3.4 Diffusion Rate Limited Oxidation

In the diffusion rate limited oxidation or diffusion controlled oxidation regime, the reactant species (oxygen) mass fractions at the wall are depleted by the surface chemical reactions ($c_{r,s} = 0$). The total mass flux of reactants to the wall are determined using the mass transfer correlations. Using equations 2.08 and 2.09,

$$\dot{m}_{(\phi)} = \sum_{r=1}^{R} \dot{m} \, c_{r,t} = -\sum_{r=1}^{R} c_{r,e} \, g_{H_r} \qquad (3.09)$$

where $\dot{m}_{(\phi)}$ is the elemental mass flux of oxygen to the wall. The net mass flux of products of oxidation reactions injected into the boundary layer must satisfy the conservation of elemental oxygen at the wall given by

$$\dot{m}_{(\phi)} + \sum_{j=1}^{J} \mathcal{M}_{\phi,j}\ \dot{m}_j = 0 \qquad (3.10)$$

and the elemental flux of surface solid phase species S which is being depleted by the oxidation process is

$$\dot{m}_D = \dot{m}_{(C^s)} = \sum_{j=1}^{J} \mathcal{M}_{S,j}\ \dot{m}_j \qquad (3.11)$$

In these expressions the quantities $\mathcal{M}_{\phi,j}$ and $\mathcal{M}_{S,j}$ are formation matrices which specify the mass concentration of ϕ and S present in the jth product species.

As an illustration, consider the simple oxidation reaction*

$$\tfrac{1}{2}\ O_2 + C^s \longrightarrow CO \qquad (3.12)$$

then

$$\mathcal{M}_{(\phi,CO)} = \frac{\mathcal{M}_{(O)}}{\mathcal{M}_{(CO)}} = \frac{16.0}{28.011} \qquad (3.13a)$$

$$\mathcal{M}_{(C^s,CO)} = \frac{\mathcal{M}_{(C^s)}}{\mathcal{M}_{(CO)}} = \frac{12.011}{28.011} \qquad (3.13b)$$

where C is the solid phase species (carbon) at the wall. The surface degradation rate due to the oxidation in this instance is given by†

$$\dot{m}_D = \dot{m}_{(C^s)} = \frac{12.011}{16.00}\ \rho_{O_2,e}\ g_{M_{O_2}} \qquad (3.14)$$

*For complex chemical oxidation reactions (i.e.: more than one product species is formed) the magnitude of the chemical kinetic rates or equilibrium chemistry constraints will determine the proportion of product species formed.

†The result shown in equation 3.14 is in exact agreement with the published results of Scala and Gilbert[13] obtained for carbon ablation.

If both 0 and 0_2 are present at the outer edge of the boundary layer the result is

$$\dot{m}_D = \dot{m}_{(C^s)} = \frac{12.011}{16.00}\left(\kappa_{O,e}\, g M_O + \kappa_{O_2,e}\, g M_{O_2}\right) \quad (3.15)$$

The total mass ablation rate of the surface material in the diffusion controlled regime is equal to the sum of the surface degradation rate of solid species entering the oxidation chemical reactions and the degradation rate due to mechanical removal (erosion) of other solid phase species which are the constituents of the surface. In this report it will be hypothesized that the mechanical removal rate is proportional to the degradation rate of the solid phase species which enter in the oxidation reactions. As an example

$$\dot{m}_c = \dot{m}_{(C^s)} + \dot{m}_{(\tilde{F})} = \dot{m}_{(C^s)} \frac{1}{\kappa_{C^s}} \quad (3.16)$$

where

$\dot{m}_c$ = the total mass ablation rate for the surface

$\dot{m}_{(\tilde{F})}$ = the mechanical removal (erosion) degradation rate of surface material

κ_{C^s} = the mass fraction of the solid phase reactant species of the surface constituents

For determining the surface mass ablation rate the mass transfer conductances of reactant species (oxygen) must be evaluated. These conductances will be affected by the magnitude of the total mass injection rate into the boundary layer. For simple ablators the total mass injection rate is equal to the surface mass ablation rate (equation 3.16). In the presence of pyrolysis products gas injection (i.e., pyrolytic ablators), the reactant species at the outer edge of the boundary layer must diffuse towards the wall against the larger mass average velocity flux of pyrolysis and ablation products. This results in a reduced mass rate of oxidizer species available to enter into the surface oxidation chemical reactions and less surface degradation in comparison with the simple ablator limiting case. The calculation of the species mass transfer conductances in the present formulation (equation 2.08 through 2.12 and 3.09 through 3.16) can be

performed by the method of successive approximations. In general

$$\dot{m} = \dot{m}_c + \dot{m}_g \tag{3.17}$$

However, in the first approximation, the surface degradation rate may be neglected in calculating the mass transfer conductance of the oxidizer species (assume $\dot{m}_c = 0$ and obtain g_{M_r} using equations 2.08 through 2.12). The first approximation of the surface ablation rate can next be calculated (e.g.: equation 3.15). In the successive approximations the preceding calculation of the surface mass ablation rate (equation 3.17) is used together with the appropriate transferred state mass fractions. Generally two or three iterations suffices to obtain adequate engineering accuracy. As an illustration, computations performed for the ablation of carbon (graphite) using the present method (C^s, CO, O_2, and N_2 species) are presented and compared with the published data of Scala[13] in Table 2.

TABLE 2 - DIFFUSION RATE CONTROLLED OXIDATION OF CARBON (GRAPHITE)

	Present Work (2 Iterations)	Scala[13]
Mass Fraction of CO $\kappa_{CO,s}$	.35545	.3498
Effective Mass Fraction of C^s $\kappa_{C,s}$	.152415	.15
Mass Transfer Blowing Parameter $B_{M_{O_2}}$	0.175118	.175

where: $$B_{M_{O_2}} = \left[\frac{\kappa_{i,e} - \kappa_{i,s}}{\kappa_{i,s} - \kappa_{i,t}}\right]_{O_2}$$

3.5 Transition Regime

For the transition regime (see Figure 4) the relation suggested by Scala[13]

$$\dot{m}_c = \left[\dot{m}_K^{-2} + \dot{m}_D^{-2}\right]^{-1/2} \tag{3.18}$$

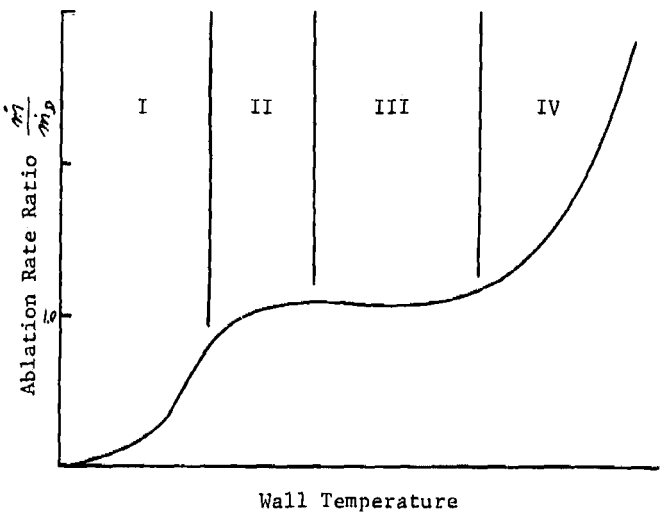

A - Ablation Rate Dependency on Temperature

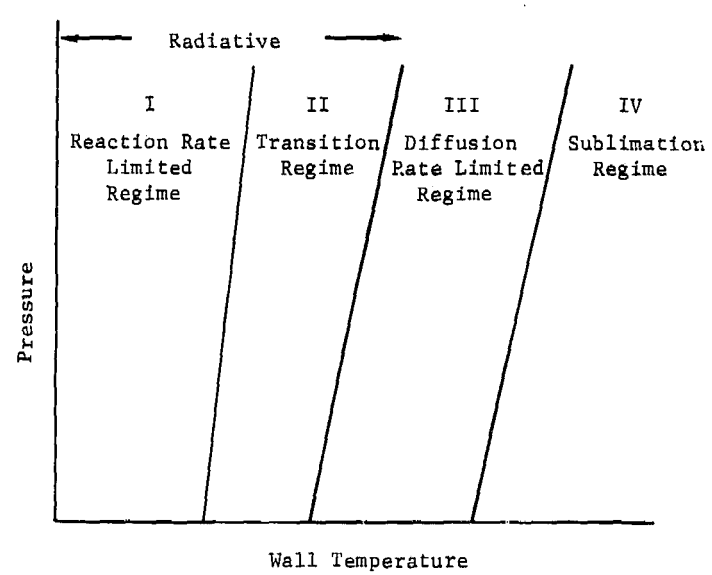

B - Ablation Regimes Dependency on Temperature and Pressure

FIGURE 4 - ABLATION REGIMES

is considered satisfactory. The mass fluxes $\dot{m}_K$ and $\dot{m}_D$ are obtained from equations 3.07 and 3.15 respectively.

3.6 Complex Ablator

The ultimate objective of the Gomez-Mills heat and mass transfer correlations[3,4] is to provide an efficient numerical model for the coupling of the boundary layer thermochemistry with a heat shield response computer program. The boundary layer thermochemistry is represented by the correlations together with a zero mass injection aerodynamic heating calculation. The coupling between the boundary layer and the heat shield response is achieved via an open system surface thermochemistry computer code. The many advantages realizable over all other ablator numerical solution procedures are:

1. A generalized representation of the boundary layer thermochemistry is achieved.
2. The surface (wall) chemical reactions may be equilibrium or/and nonequilibrium.
3. In evaluating the aerodynamic heat blockage the contribution of injectant species and outer edge reactants diffusing toward the wall are considered (e.g.: oxygen diffusing from the outer edge of the boundary layer towards the wall).
4. The surface recession rate is calculated based on the generalized surface thermochemistry model (both forward and backward reaction rates can be properly accounted for in the surface recession calculation).
5. The surface energy balance which yields the heat shield input conduction flux is calculated with greater accuracy (in this instance the heat of oxidation and heat of sublimation appearing in the energy balance are calculated considering as many molecular species and as many as desired condensed phase species).

The manner in which the correlation equations have been used in coupling the boundary layer to the surface state thermochemistry calculation is as follows.[14] First, assuming that a quasi-steady state of ablation prevails at the surface (i.e.: the time dependent derivatives in the conservation equations at the surface and in the boundary layer are neglected), the wall surface temperature and the

pyrolysis gas* injection rate at the U surface (see Figure 3) are known a priori and, hence, they are inputs to the calculation. Note that these two quantities depend on the heat shield response to the time integrated heat rate input for the entire trajectory from the initiation of reentry. Second, the objective of the calculation is to determine the corresponding conduction heat transfer rate into the heat shield and the char recession rate. In functional form, the equations used to determine these two quantities are

$$\dot{q}_{HS} = F\left(\dot{m}_g,\ p,\ T_w,\ \kappa_{i,t}\right)_s - \varepsilon\sigma T_w^4 + \dot{q}_R\left(1-\rho_R\right) \qquad (3.19)$$

$$\dot{s} = \frac{1}{\rho_c}\ F\left(\dot{m}_g,\ p,\ T_w,\ \kappa_{i,t}\right)_s \qquad (3.20)$$

where $\kappa_{i,t}$ are the mass fractions in the transferred state evaluated at the S surface for all the species considered ($i = 1 \rightarrow \nu$). These are determined from the surface state thermochemistry calculation via the mass transfer conductance correlation. Here

$$\frac{\kappa_{i,e} - \kappa_{i,s}}{\kappa_{i,s} - \kappa_{i,t}} = \frac{\dot{m}}{g_{M_i}} = B_{M_i} \qquad (3.21)$$

$$g_{M_i} = \rho_e u_e S_{T_H}^{*}\, Le_i^{0.72}\, G_M\left(a_M, B_H\right) \qquad (3.22)$$

$$a_M = F\left(M_i,\ \kappa_{i,t}\ ;\ i=1,\nu\right) \qquad (3.23)$$

where the only new unknowns are the total mass injection rate $\dot{m}$ and the mass fractions at the wall (evaluated at the S surface) $C_{i,s}$. Note that the aerodynamic heating for zero mass injection is assumed a known quantity.

Third, to initiate the surface state thermochemistry calculation, the pressure, the temperature, and the normalized pyrolysis gas injection rate are required. The latter is defined by

$$B_g' = \frac{\dot{m}_g}{\rho_e u_e S_{T_M}^{**}} \qquad (3.24)$$

* In the present generalized analytical treatment of the complex ablator, all gas phase species originating from the in-depth decomposition of the heat shield material or mechanically injected through a porous wall are termed pyrolysis gas (e.g.: pyrolytic ablators, transpiration cooling, etc)

where $\rho_e u_e St_M^{**}$ is given by the mass transfer conductance correlation

$$\rho_e u_e St_M^{**} = \rho_e u_e St_H^{*} \; Le_i^{0.72} \; G_M(a_M, B_H) \left[F_i^{2/3} \sum_{k=1}^{\nu} \frac{\kappa_{k,s}}{F_k} \right] \tag{3.25}*$$

and is the normalized mass transfer Stanton Number. This relation provides information on the relation which exists between each species' diffusive flux and the molecular composition at the wall. Accordingly,

$$\frac{\rho_e u_e St_M^{**}}{g_{M_i}} = F_i^{2/3} \sum_{k=1}^{\nu} \frac{\kappa_{k,s}}{F_k} \tag{3.26}$$

$$\rho_e u_e St_M^{**} = \frac{j_{i,s}}{\kappa_{i,e} - \kappa_{i,w}} \left[F_i^{2/3} \sum_{k=1}^{\nu} \frac{\kappa_{k,s}}{F_k} \right] \tag{3.27}$$

The surface state thermochemistry calculation provides the thermodynamic and chemical constraints required to complete the system of equations to be solved. This calculation provides the relationships which exist between

$$B_c' = \frac{\dot{m}_c}{\rho_e u_e St_M^{**}} = F(p, T_w, B_g') \tag{3.28}$$

The wall ablation mass injection rate is then

$$\dot{m}_c = B_c' \rho_e u_e St_M^{**} \tag{3.29}$$

The number of equations to be solved simultaneously is indeed large. Nevertheless, using past calculated values for the slowest changing variables, they may be easily solved by numerical methods under the quasi-steady state approximation.

4. Regenerative Cooled Heat Shields

4.1 Analytical Model

The wing leading edge skin is assumed to be thin and constructed with

*F_i = diffusion factors, see Section 6

small orifices or passages where the coolant flows in the manner illustrated in Figure 5. Because the skin is assumed to be thin, the time dependent heat storage capacity of the skin material is negligible and the skin or wall temperature corresponds to the equilibrium temperature. The coolant passage time interval is assumed small ($\Delta t \leq 0.10$ seconds) in comparison with the time variation of the trajectory parameters. Hence, the quasi-steady approximation for the coolant flow is assumed to be valid and time dependent derivatives will be assumed to be negligible. The governing equations for the analytical model described are as follows:

Energy Balance

$$\dot{q}_w - \dot{q}_{RR} = \dot{q}_F \tag{4.01}$$

where

$$\dot{q}_w = \dot{q}_{c,s}^{*} = \dot{q}_{cw\,(T_{REF})} \left(\frac{H_r - h_{w\,(T_w)}}{H_r - h_{w\,(T_{REF})}} \right)_{air} \tag{4.02}$$

$$\dot{q}_{RR} = \varepsilon \sigma T_w^4 = q_{RR\,(T_{REF})} \left(\frac{T_w^4}{T_{REF}^4} \right) \tag{4.03}$$

$$\dot{q}_F = h_f \left[h_{(T_w)} - h_{(T_b)} \right]_{COOLANT} \tag{4.04}$$

In the present formulation, the incident radiation q_r has been assumed negligible (equation 4.01). The new quantities T_b and h_f are the coolant flow bulk temperature and the skin-coolant film heat transfer coefficient.

Coolant Conservation Equations

Let a and b be the dimensions of a constant cross-section rectangular shaped orifice (Figure 5). Then assuming one dimensional steady flow:

Continuity

$$\frac{1}{\rho} \frac{d\rho}{dx} + \frac{1}{V} \frac{dV}{dx} = 0 \qquad (\rho V = \text{CONSTANT}) \tag{4.05}$$

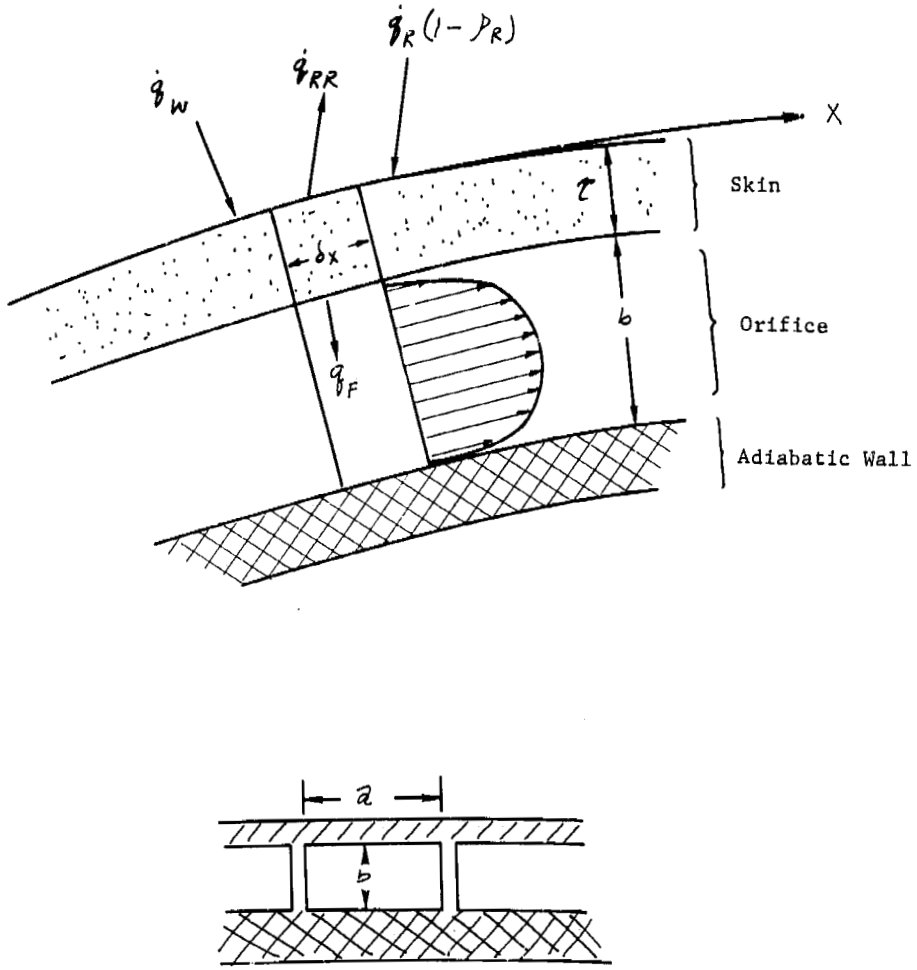

FIGURE 5 - REGENERATIVE COOLING MODEL

Momentum

$$\rho V \frac{dV}{dx} = -\frac{dp}{dx} - 2\tau_w \left(\frac{1}{a} + \frac{1}{b}\right) \qquad (4.06)$$

Energy

$$ab\,\rho V \frac{dH}{dx} = a\,\dot{q}_F + \frac{2\tau_w V}{J}(a+b) \qquad (4.07)$$

In the present notation, V is the coolant flow bulk velocity, τ_w is the average shear stress at the wall, H is the coolant stagnation enthalpy and J = 778 ft-lbf/Btu. By defining the mass flow rate per unit span as

$$\dot{m} = \rho V b \qquad (4.08)$$

and assuming

$$\frac{dH}{dx} = \frac{d}{dx}\left(h + \frac{V^2}{2Jg}\right) \simeq \frac{dh}{dx} \qquad (4.09)*$$

the conservation equations may be written in the following form

$$\dot{m} = \text{CONSTANT} \qquad (4.10)$$

$$\frac{dV}{dx} = \frac{b}{\dot{m}}\left[-\frac{dp}{dx} - \frac{2\tau_w}{b}\left(1 + \frac{1}{a/b}\right)\right] \qquad (4.11)$$

$$\frac{dh}{dx} = \frac{1}{\dot{m}}\left[\dot{q}_F + \frac{2\tau_w V}{J}\left(1 + \frac{1}{a/b}\right)\right] \qquad (4.12)$$

Equation of State

1. Caloric

$$h = \int_{T=298^\circ K}^{T} c_p\, dT + \Delta h_f \qquad (4.13)$$

2. Thermal

$$p = \rho \frac{R}{M} T \qquad \text{(for gaseous phase)} \qquad (4.14)$$

* For diatomic-rigid dumbell molecule gaseous species (e.g.: O_2, N_2, etc) the difference between the stagnation and static enthalpies is within 10% at flow Mach Numbers equal or less than 0.707.

or

$$\rho = \text{CONSTANT} \qquad \text{(for liquid phase)} \tag{4.15}$$

Forced Convection Heat Transfer Equations

Steady, variable property, pipe flow theory[15] is assumed applicable to the present problem. Above a Reynolds Number of 2,500 the flow in the pipe is turbulent and the following turbulent heat transfer correlations apply:

$$St_H = \frac{Nu}{Re\ Pr} = \left[\frac{0.0384}{Re^{1/4} + 1.8\ Re^{1/8}\ (Pr - 1)}\right]_{T^*} \tag{4.16}$$

$$\left[St_H\ Pr^{2/3}\right]_{T^*} = \frac{1}{2}\left[C_f\right]_{T^*} \tag{4.17}$$

which are evaluated at the reference temperature T^* given by

$$T^* = T_b - \frac{0.1\ Pr + 40}{Pr + 72}\left(T_b - T_w\right) \tag{4.18}$$

From equations 4.16 and 4.17, the film heat transfer coefficient h_f and the shear at the wall is obtainable

$$h_f = \rho_{(T^*)}\ V\ St_H \left[\frac{h_{(T_w)} - h_{(T^*)}}{h_{(T_w)} - h_{(T_b)}}\right]_{COOLANT} \tag{4.19}$$

$$\tau_w = \frac{1}{2}\rho_{(T^*)}\ V^2\ C_f \tag{4.20}$$

The Reynolds Number appearing in equation 4.16 is calculated according to

$$Re = \left(\frac{\rho\ V\ D}{\mu}\right)_{T^*} \tag{4.21}$$

where D is the effective diameter for a generalized cylindrical shaped pipe. According to Kreith[16]

$$D = 4 \frac{\text{AREA}}{\text{PERIMETER}} = 2b \left(\frac{a/b}{1 + a/b} \right) \tag{4.22}$$

For laminar flow in the pipe, Reynolds Number $< 2{,}500$

$$St_H = \frac{N_u}{R_e P_r} = \frac{4.12}{R_e P_r} \tag{4.23}$$

$$\frac{C_f}{2} = St_H \tag{4.24}$$

Together with equations 4.19 and 4.20, the last two equations are sufficient for determining the film heat transfer coefficient and the wall shear in the laminar flow regime. In addition, the reference temperature (equation 4.18) is not applicable (i.e.: $\tilde{T^*} = T_b$ is assumed).

4.2 Solution Procedure

The calculation of the streamwise variation of the skin temperature is performed numerically by trial and error using a finite difference procedure. In the first iteration, the initial boundary conditions of the problem are prescribed

$$T_w = T_b \tag{4.25}$$

Pressure p

Mach Number (gaseous flows)

a/b

from which the initial flow velocity and density are determined. The depth of the coolant passage is estimated using

$$\dot{m} = \rho V b = \frac{\int_{x_i}^{x_f} q_{cw}\, dx}{h_{(x_i)} - h_{(x_f)}} \tag{4.26}$$

where $h_{(x_f)}$ is an estimate of the enthalpy of the coolant at the end of the passage. Calculations at each successive streamwise step proceeds as follows:

1) At the preceding streamwise step, the temperature gradient, pressure gradient, and velocity gradient of the coolant flow are calculated using the conservation equations and the equation of state (equations 4.05 through 4.15). Then

$$T_b = T_b' + \left(\frac{dT_b}{dx}\right)' \delta x \tag{4.27a}$$

$$p = p' + \left(\frac{dp}{dx}\right)' \delta x \tag{4.27b}$$

$$V = V' + \left(\frac{dV}{dx}\right)' \delta x \tag{4.27c}$$

where the primed quantities are evaluated at the preceding streamwise step.

2) Since the film heat transfer coefficient h_f varies much slower along the streamwise coordinate than the boundary layer heat transfer rate, the preceding step value of h_f will be used in the energy balance. Then

$$\dot{q}_w = \dot{q}_{cw}\left[\frac{H_r - h_w(T_w') - c_p'(T_w - T_w')}{H_r - h_w(T_{REF})}\right]_{air} = C_1 - C_2 T_w \tag{4.28}$$

$$\dot{q}_{RR} = \frac{\dot{q}_{RR}(T_{REF})}{T_{REF}^4} T_w^4 = C_3 T_w^4 \tag{4.29}$$

$$\dot{q}_F = h_f'\left[h(T_w') + c_p'(T_w - T_w') - h(T_b)\right]_{Coolant} = C_4 + C_5 T_w \tag{4.30}$$

leads to

$$T_w^4 + \beta T_w = \alpha \qquad (4.31)$$

where

$$\beta = \frac{C_2 + C_5}{C_3}$$

$$\alpha = \frac{C_1 - C_4}{C_3}$$

Equation 4.31 can easily be solved for T_w by the method of successive approximations (e.g.: Newton-Raphson)

3) The temperature, pressure, and velocity gradients are calculated using the solution for the skin temperature at the present step. The value of the film heat transfer coefficient h_f which will be used in the next step is calculated using equation 4.19. Next go back to 1) for the next step finite difference calculation.

Although the solutions obtained in each trial calculation which correspond to a given set of initial inlet conditions are valid, the solutions may prove to be inadequate for the entire length of the coolant passages. For example, it may be desirable that the bulk flow pressure should not fall below a prescribed minimum value or that the bulk flow Mach Number should not exceed unity in order not to choke the flow (i.e.: for gaseous coolants). Therefore, for each trial calculation, a test is performed on the prescribed constraints which lead to satisfactory solutions after each streamwise step calculation is completed. If it fails to pass the test, a new trial calculation is initiated with slightly different initial boundary conditions, e.g: the inlet pressure $p_n = 1.10\ p_{m-1}$.

5. Transpiration Cooled Heat Shields

5.1 Porous Matrix Model

The porous matrix flow model equations used in the present investigation are based on the formulation of Gomez[17,18] which borrows

heavily on the investigation of Koh and del Casal[19,20] and to a lesser extent on the contributions of other contemporary investigators (e.g.: 21, 22). In the application of transpiration cooling theory to the reentry environment of interest, it was determined that the continuum laminar flow regime together with the assumption of negligible viscous dissipation adequately portrays the physics of the problem. The last restriction implies that the injectant flow rate is not too large.* Note that in the limit of massive injection through the porous matrix this assumption is no longer valid but is conservative for the transpiration cooling system integrated coolant expenditure calculation in that larger injectant flow rates will be obtained using the present formulation. Recall that large heat addition to the injectant or large viscous dissipation in the matrix (which characterizes the two limits of small and massive injection) have the same overall effect, they tend to reduce the mass injection rate. Under the preceding restrictions, the porous matrix flow governing equations are:

MOMENTUM CONSERVATION

$$\nabla p + \frac{1}{\Gamma_1}\left(\frac{\mu_i}{\rho_i}\right)\vec{\dot{m}} + \frac{1}{\Gamma_2}\,\vec{\dot{m}}\left(\nabla\cdot\left[\frac{\vec{\dot{m}}}{\rho_i}\right]\right) = 0 \qquad (5.01)$$

ENERGY CONSERVATION**

$$\nabla\cdot(-K_m\nabla T) + \nabla\cdot(\vec{\dot{m}}\,h_i) + \rho_m C_{v_m}\frac{\partial T_m}{\partial t} = \Phi = 0 \qquad (5.02)$$

$$\nabla\cdot(\vec{\dot{m}}\,h_i) = h_f^{v}(T_m - T_i) \qquad (5.03)$$

MASS CONSERVATION

$$P\left(\frac{\partial \rho_i}{\partial t}\right) - \nabla\cdot(\vec{\dot{m}}) = 0 \qquad (5.04)$$

*Moderate injection rates for the matrix are not equivalent to small blowing rates into the outer flow (the boundary layer).

**The dissipation term or shear work is given by

$$\Phi = \frac{1}{J}\left(\frac{\vec{\dot{m}}}{\rho_i}\right)\cdot\nabla p \doteq \frac{1}{J\,\Gamma_1}\,\frac{\mu_i}{\rho_i^{2}}\left(|\vec{\dot{m}}|\right)^{2}$$

It appears as a source term in the energy conservation equation. For transpiration cooling at moderate injection rates it is assumed negligible.

where:

p	pressure
μ_i	absolute viscosity for the injectant
h_f^v	volumetric film heat transfer coefficient
P	area based porosity coefficient
Γ_1 , Γ_2	permeability parameter coefficients
t	time
$\vec{m}$	vector mass flux for the injectant (lbm/ft^2-sec)
ρ_i , T_i , h_i	density, temperature, and enthalpy of the injectant
ρ_m, C_{v_m} , T_m	density, specific heat, and temperature of the matrix

The presence of transverse mass and energy fluxes is taken into account in the preceding equations but the viscous dissipation term has been omitted from the conservation of energy equation. Application of dimensional analysis to the preceding equations yields the following dimensionless similarity parameters or scaling factors:

$$f_1 = \left\{ \frac{\rho_m C_{v_m} \tau^2}{\Delta t \; k_m} \right\}_w = \frac{\text{matrix energy storage rate}}{\text{matrix conduction heat flux rate}} \qquad (5.05a)$$

$$f_2 = \left\{ \frac{\Gamma_1 \; |\vec{m}|}{\Gamma_2 \; \mu_i \; \tau} \right\}_w = \frac{\text{inertial resistance}}{\text{viscous resistance}} \qquad (5.05b)$$

$$f_3 = \left\{ \frac{h_i \; |\vec{m}|}{h_f^v \; \tau \; T_m} \right\}_w = \frac{\text{temperature difference between injectant and matrix}}{\text{temperature of the matrix}} \qquad (5.05c)$$

$$f_4 = \left\{ P \right\} = \frac{\text{injectant time dependent compressibility}}{\text{injectant steady state flow}} \qquad (5.05d)$$

where the quantities Δt and τ are conveniently chosen characteristic scaling dimensions for the time interval and the matrix thickness. For the reentry application these are of order $\Delta t \approx 100$ seconds and $\tau \approx 0.01$ ft.

For applications where the magnitude of the preceding scaling similarity parameters $\xi_1, \xi_2, \xi_3, \xi_4$ are much smaller than unity*, the approximate simpler form for the matrix flow conservation equation is:

$$-\nabla p = \frac{1}{\Gamma_1} \frac{\mu_i}{\rho_i} \vec{m} \tag{5.06a}$$

$$\nabla \cdot (K_m \nabla T) = \nabla \cdot (\vec{m} h_i) \tag{5.06b}$$

$$\nabla \cdot (\vec{m}) = 0 \tag{5.06c}$$

These equations imply that: (i) local thermodynamic equilibrium exists between the matrix and the injectant i.e., $T_m = T_i = T$, (ii) the inertial resistance is negligible in comparison with the viscous resistance, and (iii) steady state flow prevails in the matrix.

*For typical transpiration cooled R/V applications at peak heating the magnitudes of the scaling similarity parameters are:

TABLE 3 - SCALING PARAMETERS FOR TRANSPIRATION COOLING

Scaling Parameter	ICBM		Space Shuttle	
	Liquid	Gas	Liquid	Gas
ξ_1	0.00478	0.00478	$\leq$ 0.0005	$\leq$ 0.0005
ξ_2	0.00023	0.01076	$\leq$ 0.0001	$\leq$ 0.0001
ξ_3	$\leq$ 0.001**	$\leq$ 0.001**	$\leq$ 0.001**	$\leq$ 0.001**
ξ_4	0.11	0.11	0.10	0.10

**Estimate based on Koh et al. solution [19]

For the limiting case of isothermal flow, solutions of the conservation of momentum may be obtained independently of the energy equation. In this case the governing matrix flow equations reduce to:

$$\nabla \cdot \left(\frac{\Gamma_1 \rho_i}{\mu_i} \nabla p \right) = 0 \qquad \text{(ISOTHERMAL FLOW)} \tag{5.07}$$

From Gomez's analysis[18], the porous matrix permeability coefficients are ideally related to the area based porosity P and the mean pore diameter by:

$$\Gamma_1 = \frac{d^2 P}{32} \tag{5.08a}$$

$$\Gamma_2 = \frac{15}{32} P^2 \tag{5.08b}$$

$$P = \frac{\text{OPEN AREA}}{\text{TOTAL AREA}} \tag{5.08c}$$

These expressions were derived by equating the flow through the porous matrix to one dimensional flow through variable cross sectional area capillaries of diameter d. These are exact expressions when the matrix is constructed by drilling or etching small diameter holes through solid materials. When the matrix is manufactured from sintered metal powders,

$$\Gamma_1 \sim \overline{d^2} P \tag{5.09a}$$

$$\Gamma_2 \sim P^2 \tag{5.09b}$$

$$P \sim P_v^{2/3} \tag{5.09c}$$

where: $\bar{d}$ the mean diameter of the powder particles

P_v the volume based porosity

The thermal conductivity for the porous matrix is approximately related to the area porosity by

$$K_m = K_s (1 - P) \tag{5.10}$$

where: K_s = the solid matrix material thermal conductivity (the matrix thermal conductivity for $P \to 0$)

5.2 1-D Porous Matrix Flow Solutions

One dimensional flow solutions of the coupled momentum and energy equations (5.09, 5.10, and 5.11) can be readily obtained using the matrix-injectant temperature as the independent variable. In this manner the solutions may be expressed in the general form:

$$\dot{m} = E_\tau \, \dot{m}^*_{(\theta_w, \theta_i)} \tag{5.11a}$$

$$\frac{1}{2}\left\{\frac{p_i^2 - p_e^2}{p_r^2}\right\} = E_p \, p^*_{(\theta_w, \theta_i)} \left[1 + \alpha^*_I (\dot{m}^2, \Gamma_1, \Gamma_2)\right] \tag{5.11b}$$

where: $\dot{m}^*$ and p^* are dimensionless mass injection and matrix pressure drop solutions of the conservation equations which are in turn functions of the normalized wall and inlet temperatures θ_w and θ_i . The quantity α_I^* scales the ratio of inertial resistance to viscous resistance which in the above expressions is treated simply as a first order correction (α_I^* is usually less than 0.01). The quantities E_τ and E_p are matrix and injectant property groupings which characterize the transpiration cooling design. These will be defined later. The remaining quantities shown in the equations are given by the boundary conditions of the physical problem (see Figure 6). These are:

(1) Matrix outer surface boundary conditions (the wall)

p_w , ρ_w , T_w — the injectant pressure, density, and temperature

$\dot{m}_w$ — the matrix mass injection rate into the boundary layer

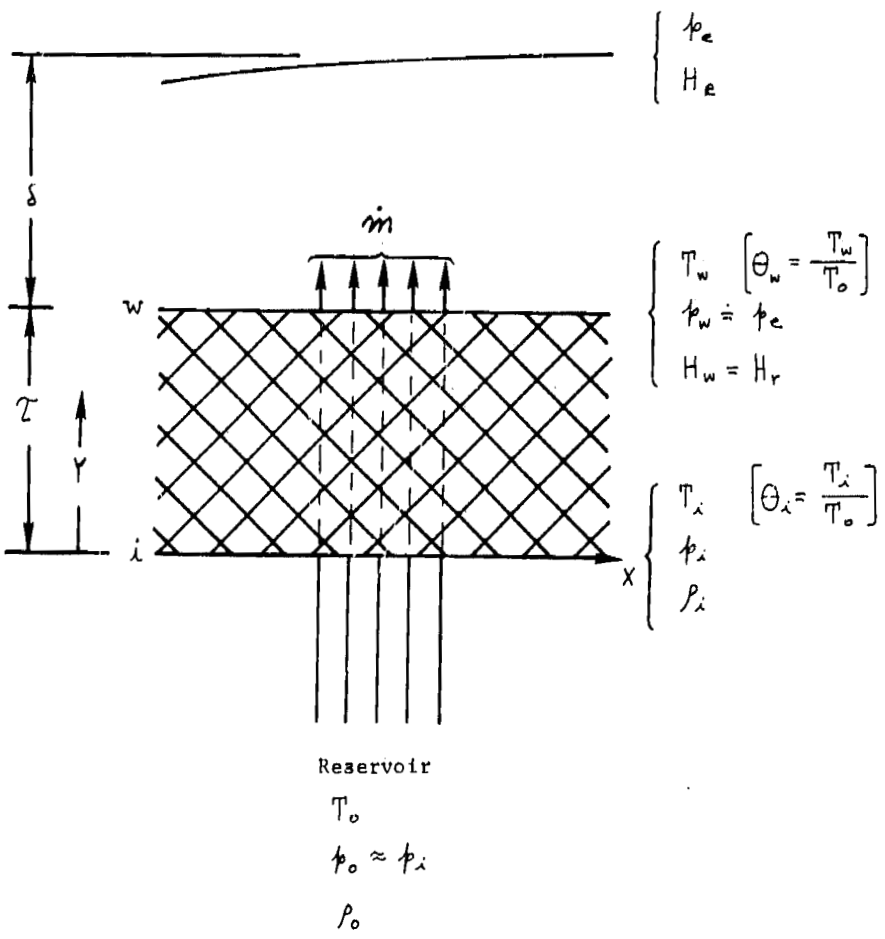

FIGURE 6 - ONE DIMENSIONAL FLOW TRANSPIRATION COOLING MODEL

(2) Matrix inner surface boundary conditions (the inlet)

p_i, ρ_i, T_i the injectant pressure, density, and temperature

(3) The reservoir (zero gradient) boundary conditions

p_o, ρ_o, T_o the injectant pressure, density, and temperature

The normalized matrix temperatures are simply:

$$\theta = \frac{T}{T_o} \quad \text{(in the matrix)} \tag{5.12a}$$

$$\theta_w = \frac{T_w}{T_o} \quad \text{(at the outer surface)} \tag{5.12b}$$

$$\theta_i = \frac{T_i}{T_o} \quad \text{(at the inner surface)} \tag{5.12c}$$

In addition, by assuming that constant pressure prevails in the matrix backface chamber (constant pressure mixing):

$$p_i \approx p_o \tag{5.13}$$

The reference pressure appearing in equation 5.11b is usually taken but not required to be equal to the reservoir pressure. The physical problem scaling factors E_τ and E_p used in the derivation of the problem dimensionless conservation equations are given by:

$$E_\tau = \frac{1-P}{\tau} \quad \frac{K_s}{C_{p_r}} \tag{5.14a}$$

$$E_p = \frac{1-P}{\Gamma_1} \quad \frac{K_s}{C_{p_r}} \quad \frac{\mu_r}{\rho_r} \quad \frac{1}{p_r} \tag{5.14b}$$

where: τ = the 1-D matrix thickness (feet)

C_{p_r}, μ_r, ρ_r = the injectant specific heat, viscosity, and density evaluated at the reference conditions (usually the reservoir conditions are used).

The dimensionless solutions of $\dot{m}^*(\theta_w, \theta_i)$ and $p^*(\theta_w, \theta_i)$ are found by integration of the conservation equations. Two classes of solutions have been considered. The first is when the injectant is assumed to be an ideal gas or an ideal liquid (incompressible) with or without a phase change in the matrix and with constant matrix properties. The second class of solutions considers the general case of arbitrary injectant and matrix properties. These solutions are only obtainable by numerical integration. In the present investigation we have devoted our attention to the solutions in the first grouping. These solutions, which are only approximate in portraying the physical problem, incorporate all the important ingredients characteristic of the flow in the porous matrix. In this manner the gross and detailed behavior of the problem will be studied.

In order to consider a liquid-vapor phase change in the analysis, it is necessary to add the definition of the following dimensionless quantities:

$$\alpha = \frac{c_{p_2}}{c_{p_1}} \tag{5.15a}$$

$$\theta_p = \frac{T_p}{T_0} \tag{5.15b}$$

$$\phi_v = \frac{\Delta h_v}{c_{p_g} T_0} \tag{5.15c}$$

$$\zeta = \alpha(\theta_p - 1) \tag{5.15d}$$

$$\epsilon_p = \frac{\phi_p}{\phi_r} \frac{M_p}{M_r} \frac{\rho_r}{\rho_p} \left[\frac{\theta_p - \phi_v - \zeta}{\theta_p}\right]^{3/2} \tag{5.15e}$$

where: $c_{p\ell}$ = injectant specific heat in the liquid phase

c_{pg} = injectant specific heat in the gas (vapor) phase

T_p = the injectant-matrix temperature at the phase change

Δh_v = the injectant heat of vaporization

p_p, ρ_p, μ_p = the injectant pressure, density, and viscosity in the gas phase evaluated at the phase change.

p_r, ρ_r, μ_r = the injectant pressure, density, and viscosity for the reference state which are chosen to correspond with the injectant properties in the liquid phase at the reservoir conditions.

The injectant properties in the liquid phase are assumed to be constant. In the gas phase, the injectant properties are adequately portrayed by ideal gas relationship as follows:

$$\frac{p_g}{p_p} = \frac{\rho_g}{\rho_p} \quad \frac{T}{T_p} \tag{5.16a}$$

$$R_g = \frac{p_p}{\rho_p T_p} \tag{5.16b}$$

$$\mu_g = \mu_p \left(\frac{T}{T_p}\right)^{1/2} \tag{5.16c}$$

Incorporating these relationships into the matrix conservation equations yields the following exact analytical solutions.

(i) Gas phase flow ($\theta_w > \theta_i \geq \theta_p$)*:

$$\dot{m}^* = LOG_e \left(\frac{\theta_w - \theta_p + \phi_v + \zeta}{\theta_i - \theta_p + \phi_v + \zeta} \right) \tag{5.17a}$$

$$p^* = \left\{ \begin{array}{l} \frac{2}{3} \left(\theta_w^{3/2} - \theta_i^{3/2} \right) + 2 \left(\theta_w^{1/2} - \theta_i^{1/2} \right) \\ + LOG_e \left(\frac{\theta_w^{1/2} - 1}{\theta_i^{1/2} - 1} \; \frac{\theta_i^{1/2} + 1}{\theta_w^{1/2} + 1} \right) \end{array} \right\} \tag{5.17b}$$

$$\alpha_I^* = \frac{\Gamma_1}{\Gamma_2} \left(\frac{\dot{m}^2}{M_p} \; \frac{1}{1-P} \; \frac{\kappa_{p_e}}{K_s} \right) \left(\frac{\theta_w - \theta_i}{p^*} \right) \tag{5.17c}$$

(ii) Phase change in the matrix ($\theta_w > \theta_p > \theta_i$):

$$\dot{m}^* = LOG_e \left\{ \left(\frac{\theta_w - \theta_p + \phi_v + \zeta}{\phi_v + \zeta} \right) \left(\frac{\theta_p - 1}{\theta_i - 1} \right)^{\frac{1}{\alpha}} \right\} \tag{5.18a}$$

$$p^* = \epsilon_p I_1 + \frac{1}{2} \frac{1}{\alpha} I_2 \left\{ E_p \frac{1}{\alpha} I_2 + 2 \sqrt{2 \epsilon_p E_p I_1 + \left(\frac{p_e}{p_r} \right)^2} \right\} \tag{5.18b}$$

where I_1 and I_2 are integrals given by:

$$I_1 = \left\{ \begin{array}{l} \frac{2}{3} \left(\theta_w^{3/2} - \theta_i^{3/2} \right) + 2 \left(\theta_w^{1/2} - \theta_p^{1/2} \right) \\ + LOG_e \left(\frac{\theta_w^{1/2} - 1}{\theta_p^{1/2} - 1} \; \frac{\theta_p^{1/2} + 1}{\theta_w^{1/2} + 1} \right) \end{array} \right\} \tag{5.18c}$$

$$I_2 = LOG_e \left(\frac{\theta_p - 1}{\theta_i - 1} \right) \tag{5.18d}$$

*For inert "gas" injectants, these equations may be written in simpler form by observing that:

$$\phi_v = 0 \quad , \quad \theta_p - \zeta = 1 \quad , \quad \epsilon_p = \alpha = \theta_p = 1$$

(iii) Liquid phase flow ($\theta_p \geq \theta_w > \theta_i$)*:

$$\dot{m}^* = LOG_e\left\{\left(\frac{\theta_w - 1}{\theta_i - 1}\right)^{1/\alpha}\right\} \tag{5.19a}$$

$$p^* = \frac{1}{2}\ \frac{1}{\alpha}\ LOG_e\left(\frac{\theta_w - 1}{\theta_i - 1}\right)\left\{\frac{E_p}{\alpha}\ LOG_e\left(\frac{\theta_w - 1}{\theta_i - 1}\right) + 2\ \frac{p_e}{p_r}\right\} \tag{5.19b}$$

---

*Note that in this generalized treatment of the problem the liquid phase solution appears more complex than it needs to be. By re-defining E_p, a simpler form of the same solution is obtained, i.e.:

$$\frac{p_i - p_e}{p_r} = E_p'\ p^{*'}(\theta_w, \theta_i) \tag{5.19c}$$

$$p^{*'} = LOG_e\left(\frac{\theta_w - 1}{\theta_i - 1}\right) \tag{5.19d}$$

5.3 Matrix Flow-Boundary Layer Coupled Behavior

In the preceding sections the 1-D matrix flow solutions and the boundary layer heat blocking correlations have been presented. These will be now considered together and their coupled behavior which characterized the transpiration cooling problem will be investigated. Inert species injectants with and without a phase change in the matrix will be considered. Chemical reactions between the injectants, the matrix, and the boundary layer edge flow species will be excluded. This simple model provides sufficient information to portray the characteristic behavior of the generalized coupled problem.

The boundary conditions will be defined in terms of the outer flow zero mass injection aerodynamic heating information and the injectant enthalpy at reservoir conditions. The matrix temperature at the outer surface (the wall) is defined as the independent variable. This is found convenient in that it simplifies the mathematical formulation of the coupled problem. The principal dependent variables will be the mass injection rate and the injectant reservoir pressure. To account for the variation of the boundary layer zero mass injection convective heat transfer rate to the wall with wall temperature, the usual enthalpy correction will be assumed:

$$\dot{q}_{c,s}^{*} = \dot{q}_{cw}\left[\frac{H_r - c_p T_w}{H_r - c_p T_{REF}}\right]_{air} = \rho_e u_e St_H^{*}\left(H_r - c_p T_w\right)_{air} \tag{5.20}$$

where: c_p = the specific heat of the edge species (air)

$\dot{q}_{cw}$ = the convective heat transfer rate for zero mass injection evaluated at some reference temperature T_R

St_H^{*} = zero mass injection boundary layer Stanton Number evaluated at the reference temperature T_R.

(h = c_pT)

The coupled problem governing equations are obtained by combining the 1-D matrix flow solutions presented earlier with the zero mass injection aerodynamic heating boundary condition (equation 5.20) via the blocking correlations and the interface energy balance (equations 1.01-1.08, and 2.01-2.07). The coupled conservation of energy equations yield the normalized matrix inlet temperature θ_i as a function of the independent variable, the normalized wall temperature θ_w , as follows:

(i) Gas phase flow $(\theta_w > \theta_i \geq \theta_p)$:

$$\theta_i = \frac{\theta_w - \theta_p + \phi_v + \zeta}{\left\{1 + \frac{B^*\left(1 - \frac{\theta_w}{Z^*}\right)}{\theta_w - \theta_p + \phi_v + \zeta}\right\}^{Q^*/B^*}} + (\theta_p - 1) - \phi_v - \zeta \qquad (5.21a)$$

(ii) Phase change in the matrix $(\theta_w > \theta_p > \theta_i)$:

$$\theta_i = \left[\frac{\frac{\theta_w - \theta_p}{\phi_v + \zeta} + 1}{\left\{1 + \frac{B^*\left(1 - \frac{\theta_w}{Z^*}\right)}{\theta_w - \theta_p + \phi_v + \zeta}\right\}^{Q^*/B^*}}\right]^{\alpha} \qquad (5.21b)$$

(iii) Liquid phase flow $(\theta_p = \theta_w > \theta_i)$* :

$$\theta_i = (\theta_w - 1)\left[\frac{1}{\left\{1 + \frac{B^*\left(1 - \frac{\theta_w}{Z^*}\right)}{\phi_v + \zeta}\right\}^{Q^*/B^*}}\right]^{\alpha} \qquad (5.21c)$$

* $T_w = T_p$ has been assumed. This requires that the coolant at the wall vaporizes at the same rate as the coolant mass injection rate through the porous wall. Therefore, the presence of a liquid film between the wall and the outer flow has been neglected.

These equations yield the coupled problem characteristic similarity parameters which are defined as:

$$Q^* = \frac{\dot{q}^*_{c,s}}{(1-P)\frac{K_s T_o}{\tau}}$$ The Matrix Nusselt Number (5.22a)

$$B^* = \frac{H_r}{\left(\frac{c_{p_v} T_o}{a_{H_2}}\right)_{air}}$$ The Injectant Blocking Number (5.22b)

$$Z^* = \frac{H_r}{(c_p T_o)_{air}}$$ The Cooling Ratio Number (5.22c)

The other dimensionless numbers appearing in the coupled equations (Θ_p, ϕ_v, ζ, α) were introduced earlier (equation 5.15). These parameters prescribe the thermodynamic properties of the injectant. The corresponding magnitudes of the normalized mass injection rate $\dot{m}^*$ and pressure drop p^* were given as a function of the matrix normalized inner and outer temperatures (Θ_w, Θ_i). Using these, it is a simple task to calculate the actual mass injection rate, pressure drop, and backface chamber pressure using the 1-D matrix flow solutions (equations 5.17, 5.18, and 5.19).

The characteristic behavior of the coupled solutions is illustrated schematically in Figure 7. The two curves presented show the variation of the normalized pressure drop p^* and mass injection rate $\dot{m}^*$ versus the matrix outer surface temperature Θ_w. In examining the figure for the first time it is surprising to find an inflection point on the pressure drop curve. This behavior can be satisfactorily explained by examining the role played by the product of the injectant kinematic viscosity and injection rate. Recall that the kinematic viscosity is an increasing function of temperature for real gases and for fluids in the vapor phase. After examining the conservation of momentum equation (equation 5.06a) it is clear that for a given pressure drop, various combinations of kinematic viscosity

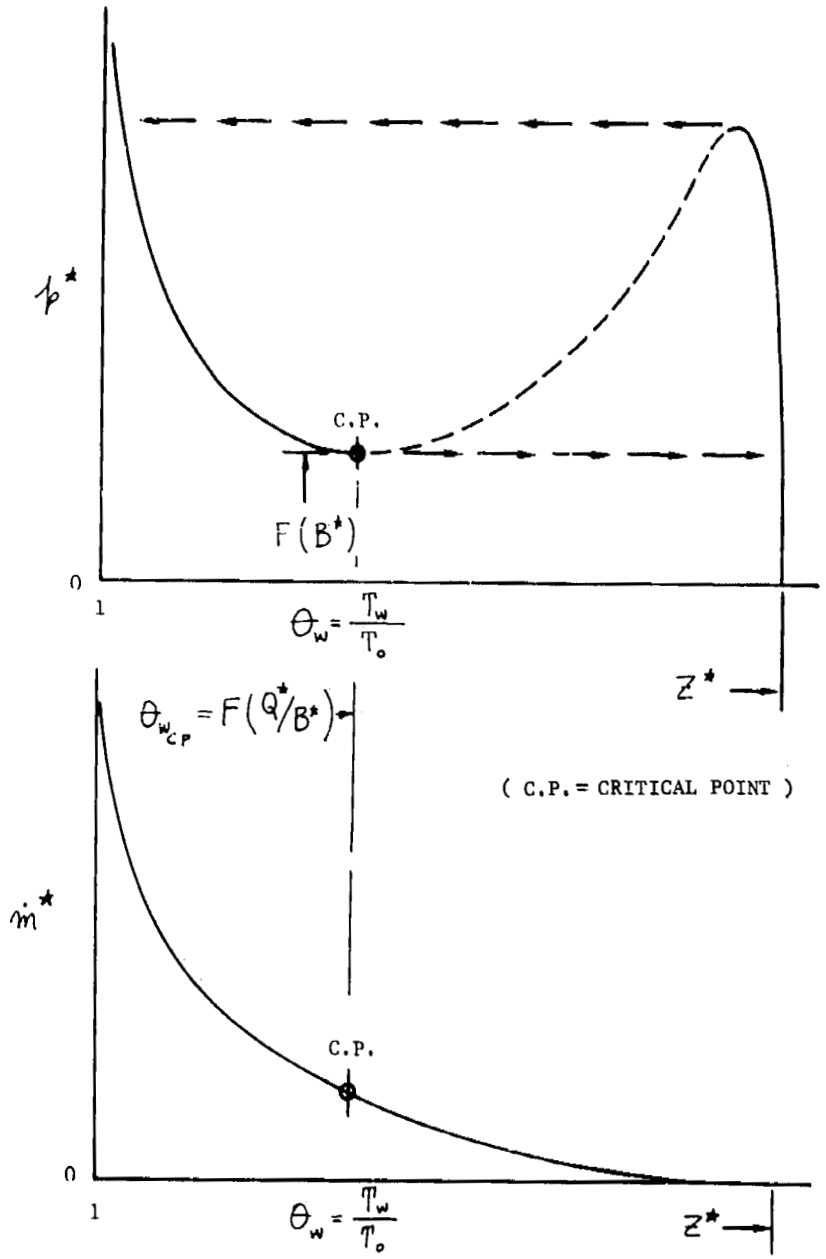

FIGURE 7 - PRESSURE DROP AND MASS INJECTION RATE DEPENDENCY ON WALL TEMPERATURE FOR 1-D TRANSPIRATION COOLING

versus mass injection rates are possible depending on the mean temperature of the matrix. This means that for a given pressure drop across the matrix, two different mass injection rates may be found which satisfy the steady state conservation equations depending on whether the matrix is hot or cold. For transpiration cooling applications the variation of the pressure drop with the mass injection rate are of great importance since the porous matrix can only be adequately protected if variations in the backface chamber pressure positively control the mass injection rate. This requirement can be clearly stated by evaluating the slope of the pressure-mass injection rate curve which must be positive

$$\frac{d p^*}{d \dot{m}^*} \geq 0 \quad \text{(For positive injection control)} \qquad (5.23)$$

When the slope is negative, injection control is lost. The steady state solutions of the coupled equations are unstable. To illustrate this point refer to the next figure (Figure 8). Here the variation of pressure drop versus the mass injection rate is presented for both ideal gas and liquid injection with a phase change. Consider an initial steady state operating point lying in the portion of the curve where the slope is negative. Then, a small step change reduction in the pressure at the backface chamber will result in a nearly instantaneous readjustment of the mass injection rate. In comparison, the time dependent matrix heat storage capacity will not permit as rapid readjustment of the matrix temperature profiles which would make it possible for the operating point to shift to the nearest steady state position on the curve. Instead the flow is going to be reduced somewhat which results in an increased heating rate into the matrix. As the matrix temperature increases, the kinematic viscosity of the injectant increases and further reductions in the mass injection rate will occur. This unsteady readjustment will continue until the operating point reaches the hot matrix steady state solution where the slope is positive. The same reasoning when applied in reverse would show an overall readjustment of the flow until the cold matrix

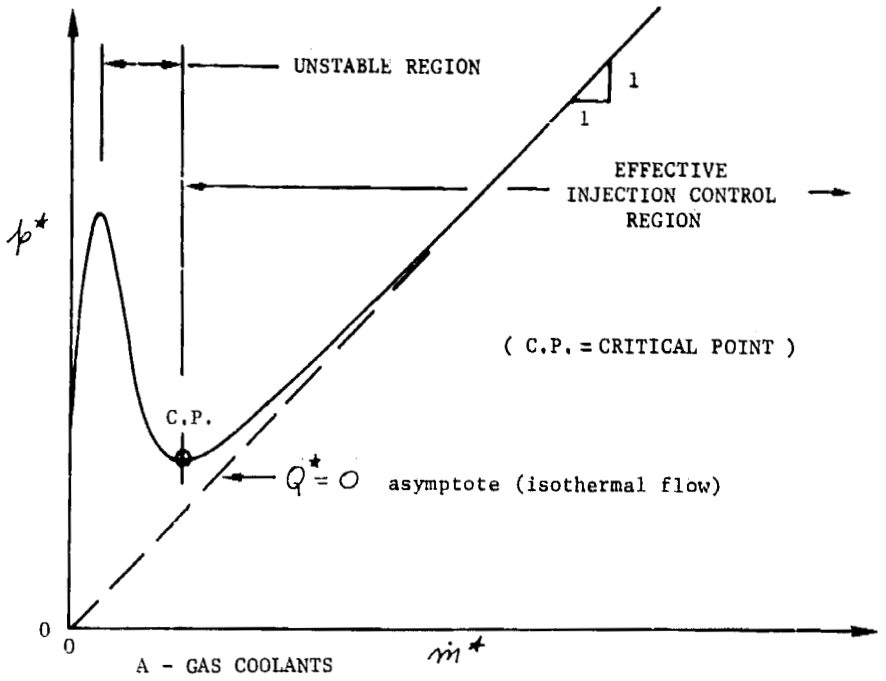

A - GAS COOLANTS

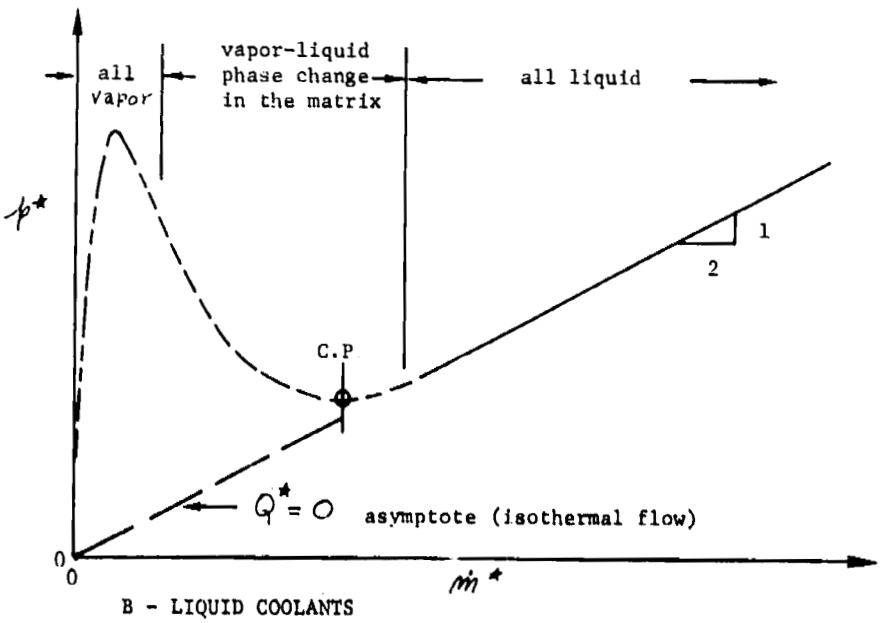

B - LIQUID COOLANTS

FIGURE 8 - PRESSURE DROP VS. MASS INJECTION RATE FOR 1-D TRANSPIRATION COOLING

steady state portion of the curve is reached. Hence where the slope is negative the steady state solutions are unstable. Another point in question is that these solutions correspond to conditions where the matrix backface heat flux into the backface chamber is too large and, hence, it is questionable if these solutions can ever be realized. Nevertheless, the slope is a measure of the magnitude of the static stability of injection control.

From the preceding discussion it is evident that for the transpiration cooling applications a given design must operate in the stable portion of the curve where positive injection control (through the variation of the backface chamber pressure) is realizable. This means that a given design must operate at mass injection rates which are larger than the mass injection rate at the critical point where the static stability slope is zero (see Figure 7). To operate at backface chamber pressures near the critical point runs the risk of losing the injection control. In this case the matrix temperature may increase and the mass injection rate decrease uncontrollably until a new steady state equilibrium point is reached where chemical reactions at the outer matrix surface (the wall) dominate the problem (i.e.: oxidation and sublimation of the matrix). This implies that the matrix temperature at the outer surface (the wall) corresponding to the critical injection falls below the matrix melting temperature. It is interesting to note that this assertion has been shown to be generally correct for the transpiration cooling reentry missions considered to date. Another point worth mentioning is that the majority of the boundary layer mass injection studies published in the literature supposedly for transpiration cooling consider a wall temperature which is too high. They invariably fall in the unstable region of injection control of the coupled problem.

The matrix outer surface (the wall) temperature and mass injection rate at the critical control point have been mapped as a function of the coupled problem similarity parameters for the entire R/V transpiration cooling range of interest when the injectant is assumed to be an ideal gas (see Figures 9 and 10). On the other hand for liquid injection, the dependency of the solution on the injectant thermodynamic

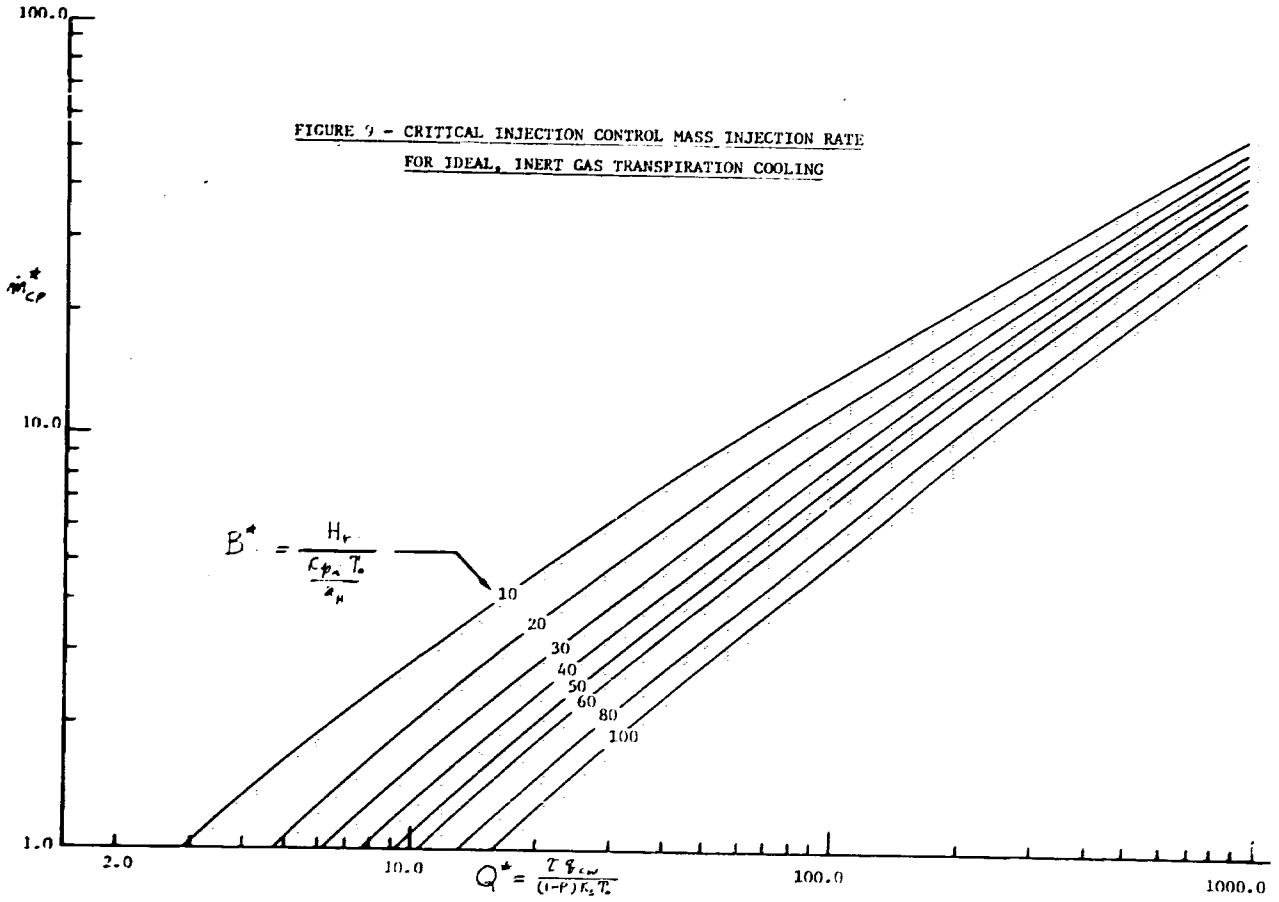

FIGURE 9 - CRITICAL INJECTION CONTROL MASS INJECTION RATE FOR IDEAL, INERT GAS TRANSPIRATION COOLING

FIGURE 10 - CRITICAL INJECTION CONTROL MATRIX WALL TEMPERATURE FOR IDEAL, INERT GAS TRANSPIRATION COOLING

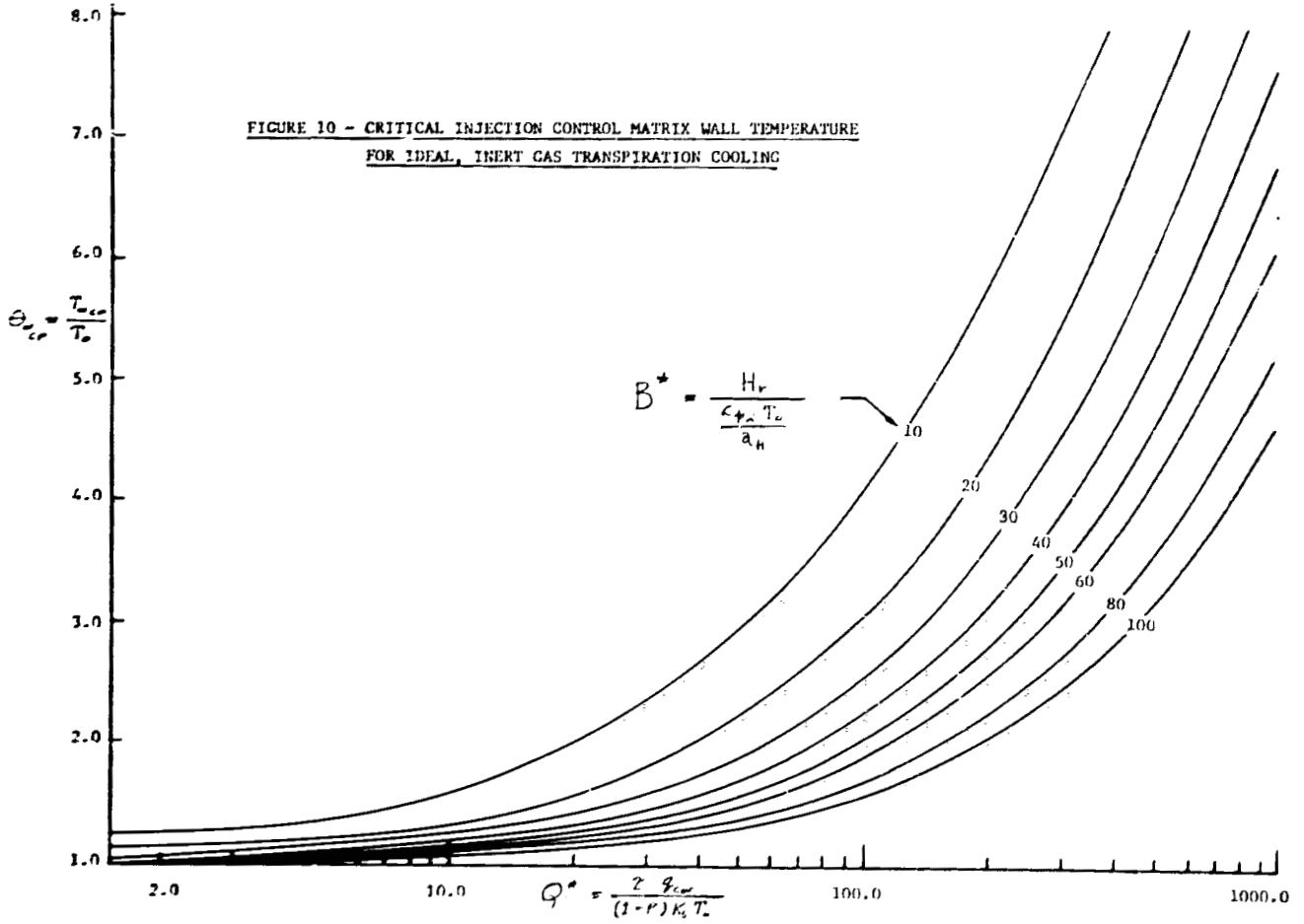

properties in the neighborhood of the phase change precludes such a generalized treatment. Nevertheless the behavior is the same as for ideal gases when a small portion of the flow in the matrix is in the vapor phase. Therefore, as long as the phase change is not allowed to occur within the matrix the flow will be stable.

The behavior of the coupled problem was also investigated using other less accurate functions of the heat blocking correlation. The results of this investigation served to illustrate the dependency of the coupled problem on the blocking correlation. These are illustrated in Figure 11. The principal conclusion drawn is that the gross behavior of the couple problem remains unchanged. On the other hand, the critical mass injection rate is shifted somewhat and hence it can be appreciated that the accuracy of the blocking correlation plays an important part in evaluating the critical operating point of the coupled problem.

5.4 Matrix Design Optimization

The optimum transpiration cooled heat shield matrix design for a selected reentry mission is by definition a configuration which will provide positive injection control and the minimum coolant (injectant) time integrated expenditure. Ideally, the absolute minimum coolant expenditure corresponds to a condition when the matrix outer surface temperature is uniform and equal to the matrix melting temperature. However, in the design of a real heat shield, this idealized condition can only be approximated at one selected time point of the reentry trajectory. Even then, the mass injection stability requirements usually prescribe a matrix maximum temperature which falls far below the matrix melting temperature. Hence the matrix configuration should be optimized at the critical peak heating reentry time point. In this manner the matrix will be operating near its optimum design point in the critical region of reentry encompassing peak heating and peak pressure where the coolant rates of expenditure are largest. This optimization criterion will provide the least time integrated coolant expenditure.

The optimization procedure for the transpiration heat shield at a selected time point of the reentry trajectory can be deduced from

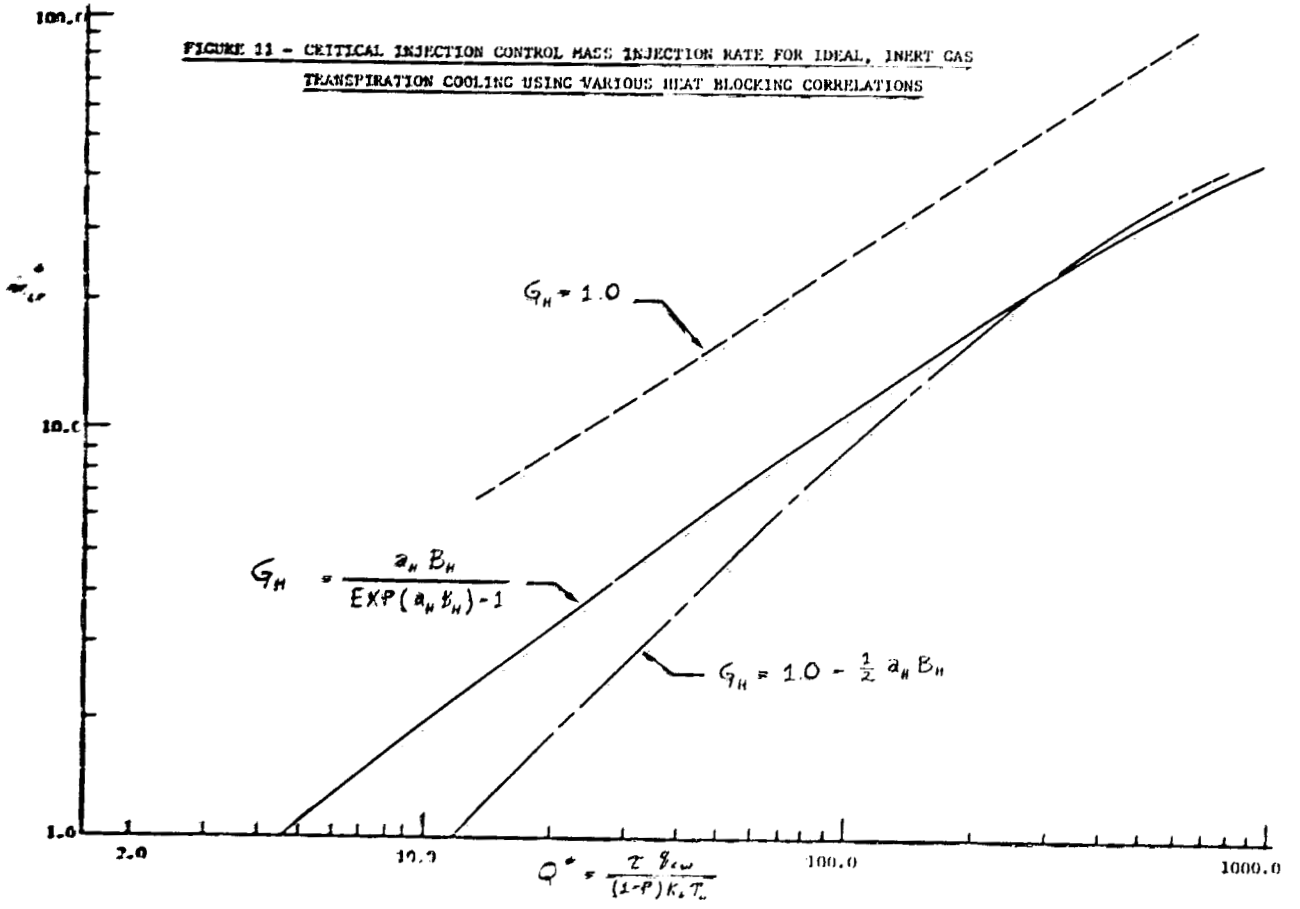

FIGURE 11 - CRITICAL INJECTION CONTROL MASS INJECTION RATE FOR IDEAL, INERT GAS TRANSPIRATION COOLING USING VARIOUS HEAT BLOCKING CORRELATIONS

the one dimensional dependent coupled problem exact analytical solutions. In order to minimize the coolant rate of expenditure, the outer surface temperature (the wall temperature) must be uniform and as large as the injection stability and/or matrix melt temperature permits. This is accomplished when the dimensionless one dimensional dependent solutions are identical for all the streamlines. A condition which arises from the fact that the backface chamber boundary conditions are common to all the streamlines. Accordingly, the dimensionless mass injection $\dot{m}^*$, pressure drop ϕ^*, and the matrix flow similarity parameters are the same for all the streamlines.

Hence the matrix temperature profiles are similar profiles. Using previous analytical results (equations 5.11, 5.17, 5.18, and 5.19) it follows:

$$\frac{\dot{q}_{c,s}^{*}(x)}{\dfrac{(1-P(x))K_s T_o}{\tau_{(x)}}} = Q^* = \text{CONSTANT} \qquad (5.24a)$$

$$\frac{\dot{m}_w(x)}{\dfrac{(1-P(x))}{\tau_{(x)}}\dfrac{K_s}{c_{p_r}}} = \dot{m}^* = \text{CONSTANT} \qquad (5.24b)$$

$$\frac{\dfrac{1}{2}\dfrac{p_s^2 - p_{e(x)}^2}{p_r^2}}{\dfrac{(1-P(x))}{\Gamma_{1(x)}}\dfrac{K_s}{c_{p_r}}\dfrac{M_r}{p_r}\dfrac{1}{p_r}} = \phi^* = \text{CONSTANT} \Big|_{\text{ideal gases}} \qquad (5.24c)$$

$$\frac{\dfrac{p_s - p_{e(x)}}{p_r}}{\dfrac{(1-P(x))}{\Gamma_{1(x)}}\dfrac{K_s}{c_{p_r}}\dfrac{M_r}{p_r}\dfrac{1}{p_r}} = \phi^{*\prime} = \text{CONSTANT} \Big|_{\text{ideal liquids}} \qquad (5.24d)$$

where X streamwise coordinate (Figure 6)

τ the one dimensional dependent solution matrix thickness

Since the variation of the area porosity P has been found to be small in the transpiration cooling range of applications ($P_{(X)} \leq 0.10$), these equations can be rewritten approximately as:

$$\frac{\tau_{(X)}}{\tau_{(X_m)}} = \left[\frac{\dot{q}_{cw}(X)}{\dot{q}_{cw}(X_m)}\right]^{-1} \tag{5.25a}$$

$$\frac{\dot{m}_w(X)}{\dot{m}_w(X_m)} = \frac{\dot{q}_{cw}(X)}{\dot{q}_{cw}(X_m)} \tag{5.25b}$$

$$\frac{P_1(X)}{P_1(X_m)} = \left\{\frac{1 - \left[\frac{p_e(X)}{p_i}\right]^n}{1 - \left[\frac{p_e(X_m)}{p_i}\right]^n}\right\}^{-1} \tag{5.25c}$$

$$\phi = \frac{p_i}{p_e(X_m)} \tag{5.25d}$$

where: $n = 2$ for ideal gas injection

$n = 1$ for ideal liquid injection

$X_m =$ x coordinate for $\dot{q}_{cw}$ maximum

From these expressions it is evident that the optimum heat shield configuration requires that the thickness* vary inversely proportional

*Note that the thickness τ is the one dimensional dependent solution matrix thickness.

to the zero mass injection heat flux to the wall. The permeability variation is a function of the external pressure and the backface chamber pressure.* For large values of design pressure ratio ϕ, the required permeability variation will be negligible.

For matrix designs which deviate from the optimum design configuration (e.g.: constant thickness,constant permeability,etc), the wall temperature distribution on the wall surface will vary. For positive injection control, the backface chamber pressure or inlet pressure must be sufficiently large to provide adequate cooling at all spatial locations on the wall surface. Under these conditions, only at one critical spatial location on the wall surface will the mass injection rate be at or near the minimum injection rate corresponding to the critical injection control point(see Figure 7 and 8). Away from this critical location, excess coolant injection or overcooling will prevail. This will result in an overall larger coolant expenditure than obtained for the optimum matrix design configuration. For liquid coolants, the mass vaporization rate of coolant species will be less than the mass injection rate at the wall at all spatial locations away from the critical location and a thin liquid film will appear and wet the wall. The presence of the liquid film and its effect on the external flow has been neglected in the analysis. Nevertheless, with respect to the wall mass injection rate distribution and the coolant expenditure, the present analysis provides valid solutions since away from the critical location the mass injection rate through the porous matrix is governed by the backface chamber pressure which is determined from the injection requirements at the critical location.

* The matrix permeability is assumed to vary in the direction parallel to the wall surface and constant in the direction normal to the wall.

6. Thermodynamic and Transport Properties

For ablation and regenerative cooling calculations, the thermodynamic and transport properties of species (i.e.: air, coolant, and ablation products) are determined in the following manner:

1. Thermodynamic Properties

Thermodynamic properties are obtained from the JANAF tables[23] and other sources[24, 25, 26] and used in the form of polynomial curve fits to the tabulated data. Constants appropriate to a lower and an upper temperature range (less or greater than 3000°K) are determined by a least squares curve-fit routine. The curve-fits are as follows with T in degrees Kelvin:

Heat of Formation at 298°K (Cal/Mole)

$$\Delta h_f = h_{298^\circ K} = F_1 \tag{6.01}$$

Heat Capacity (Cal/Mole-Deg.K)

$$c_p = F_3 + F_4 T + F_5/T^2 \tag{6.02}$$

Enthalpy (Cal/Mole)

$$h - h_{298^\circ K} = F_2 + F_3(T-3000) + 0.5\,F_4(T^2-3000^2) - F_5\left(\frac{1}{T} - \frac{1}{3000}\right) \tag{6.03}$$

Entropy (Cal/Mole-Deg.K)

$$S = F_6 + F_3 \log_e\left(\frac{T}{3000}\right) + F_4(T-3000) - 0.5\,F_5\left(\frac{1}{T^2} - \frac{1}{3000^2}\right) \tag{6.04}$$

2. Transport Properties

The viscosities and thermal conductivities of the pure components, and the reference diffusion coefficient are computed in the manner recommended by Hirschfelder, Curtiss, and Bird,[27] The Lennard-Jones interaction potential is assumed and the required parameters obtained from Svehla[28] and Hochstim.[29] The mixture

viscosity is calculated following the method of Wilke[30] and the mixture thermal conductivity according to Mason and Saxena.[31] The multi-component binary diffusion coefficients of species are calculated according to the bifurcation approximation[6]

$$\mathcal{D}_{i,j} = \frac{\overline{\mathcal{D}}}{F_i \, F_j} \tag{6.05}$$

$$F_i = \left(\frac{\mathcal{M}_i}{32}\right)^{0.461} \tag{6.06}$$

where $\overline{\mathcal{D}}$ the reference diffusion coefficient (= the self diffusion coefficient of molecular oxygen, $\mathcal{M}$ = 32)

F_i, F_j the diffusion factors of species i and j.

CONCLUSIONS

The development of analytical models and numerical solution procedures for determining the performance of three leading thermal protection design concepts for application to the space shuttle entry missions has been presented. The range of applicability and the limitations of the analysis for each design concept are as follows:

1) Radiative and Ablative Systems

The accuracy of the solutions for ablative and radiative heat shield design concepts is dependent on the following factors: (i) the availability of empirical and reliable test data for the reaction rate limited oxidation regime in the appropriate range of applications of temperature, pressure, and the oxidizing atmosphere elemental composition, and (ii) the availability of accurate thermochemical data for all molecular species which enter into the chemical reactions at the wall interface and at the boundary layer flow.

2) Regenerative Cooled Systems

The use of rocket propellants such as gaseous hydrogen and oxygen as coolants which are readily available in quantity aboard the space shuttle is envisoned to be the determining factor in the selection of coolants. In this case, accurate thermal protection solutions can be obtained only if complete and accurate information on the thermodynamic and transport properties of coolants at very low and elevated temperatures are used in the numerical solution procedures.

3) Transpiration Cooling Systems

The calculation of the coolant flow rates through the porous wing leading edge skin which are required to provide adequate thermal protection is based on the flow control injection stability requirements. For the space shuttle entry missions which are considered in this study, the zero mass injection convective heating to the exposed wing surface is many times smaller than for other entry vehicle applications for which transpiration cooling systems have been investigated.[17] Under these conditions, the major part of the convective heating is blocked by the mass injection effects and the remainder,

which is very small, is conducted into the heat shield. The amount of heat blocked ranges from 96% to ∿ 100% for representative space shuttle entry trajectories.[32] For this range of applications, the heat and mass transfer correlations on which the analysis of the heat blocking effects are based do not provide accurate predictions. As a direct result, the magnitudes of the calculated mass injection rates although very small relative to the flow in the porous matrix (i.e., the leading edge skin) are considered sufficiently large to cause the separation of the flow over the wing. Therefore, the mass injection rates and the spatial-time integrated coolant expenditure predictions using the present analytical procedure are considered to be very conservative. To improve the analysis more accurate heat and mass transfer correlations in this range of applications should be developed. Furthermore, it should be noted that the coolant thermodynamic and transport properties for the flow in the porous matrix were assumed to correspond to that of an ideal gas or an ideal liquid (i.e., incompressible). Another factor which was omitted in the analysis is the coupling which exists between entry vehicle dynamics and the mass injection effects.* This coupling which is generally neglected for ablative systems may prove to have a significant effect on the performance of the integrated transpiration cooled vehicle.

4) Discontinuities

In the analytical treatments presented, no provisions were made for determining the effects of discontinuities in the heat shield design. Such discontinuities would arise as a result of using a step change in heat shield materials for ablators or step changes in the mass injection rates for transpiration cooled heat shields. This limitation results from the use of heat and mass transfer correlations for predicting the boundary layer mass and energy fluxes to the wall which are based on the analysis of similar solutions for the stagnation region. (Step changes in the wall temperature or the mass injection rate are not permitted.)

*Large reductions in the heat transfer rate due to mass injection (the heat blocking effects) are accompanied by comparable reductions of the skin friction or friction drag.

The effectiveness of the analytical solution procedures is dependent on the accuracy in which the analytical models portray the real problem situations. On this basis, an evaluation of the solution procedures developed for the present study has led to the following conclusions: (i) the radiative and ablative systems solution procedure is considered to be the most accurate and reliable procedure, (ii) the solution procedure for the regenerative cooled systems is nearly equivalent to the procedure for the radiative and ablative systems, and, (iii) the solution procedure for the transpiration cooled systems, although the least accurate, provides conservative predictions on the coolant expenditure and an accurate portrayal of the gross behavior of the real problem.

REFERENCES

1. H. Hoshizaki, "Heat Transfer in Planetary Atmospheres at Super-Satellite Speeds," ARS Journal 32, 1544 (1962).

2. Lees, L., "Ablation in Hypersonic Flows," Seventh Anglo-American Aeronautical Conference; Institute of Aeronautical Sciences, Inc., New York, 1950, pp. 254-267.

3. Gomez, A. V., A. F. Mills and D. M. Curry, "Correlations of Heat Transfer for the Stagnation Region of a Reentry Vehicle with Multicomponent Mass Addition," ASME Paper 70-HT/SpT-21 ("Space Technology for the 70's, Part II," ASME, Sept. 1970).

4. Mills, A. F., A. V. Gomez and G. S. Strouhal, "The Effects of Gas Phase Chemical Reactions on Heat Transfer to a Charring Ablator." AIAA 5th Thermophysics Conference, Paper No. 70-869.

5. Spalding, D. B., "A Standard Formulation of the Steady Convective Mass Transfer Problem," Int. J. Heat. Mass Transfer, Vol. 1, pp. 192-207, Pergamon Press, 1960.

6. Kendall, R. M., Bartlett, E. P., Rindal, R. A., and Moyer, C. B., "An Analysis of the Coupled Chemically Reacting Boundary Layer and Charring Ablator," NASA CR 1060, 1968.

7. R. W. Detra, N. H. Kemp, and F. R. Riddell, "Addendum to Heat Transfer to Satellite Vehicles Reentering the Atmosphere," Jet Propulsion 27, 1256 (1957).

8. Gomez, A. V., "Hypersonic-Blunt Body, Shock Layer Analysis Program (HA002A)", TRW IOC 70.4352.30-02, February 1970.

9. E. P. Bartlett and R. M. Kendall, "Non-Similar Solution of the Multicomponent Laminar Boundary Layer by an Integral Matrix Method," Aerotherm Report No. 66-7, Part III, Palo Alto, 1967 (NASA CR-1062, June 1968).

10. Wilkinson, H. R. and G. H. Heimler, "Aerodynamic Surface Heating Program (AH005H)", TRW Report 67.3123.22-172, October 1967 and Revisions up to July 1969.

11. Miller, B., "Thermal Analysis of the Proposed NASA/MSC Shuttle Wing Design", TRW IOC 69.4352.20-6.

12. Ong, J. N., Jr., "Oxidation of Refractory Metals as a Function of Pressure, Temperature and Time: Tungsten in Oxygen," J. Electrochemical Society, Vol. 9, No. 4, April 1962, pp. 284-288.

13. Scala, S. M. and L. M. Gilbert, "Sublimation of Graphite at Hypersonic Speeds," AIAA Journal, Vol. 3, No. 9, September 1965.

14. Gomez, A. V. and A. F. Mills, "Multi-Component, Foreign Species Injection, Heat Transfer, Skin Friction, and Mass Transfer Correlations for the Hypersonic, Laminar Boundary Layer in the Stagnation Region Including Chemical Reactions," TRW Report No. 11176OH244-RO-00, 30 June 1969.

15. Eckert, E.R.G. and Drake Jr., R. M., "Heat and Mass Transfer," McGraw Hill, New York, Second Edition, 1959, pp. 167-228.

16. Kreith, Frank, "Principles of Heat Transfer," International Textbook Co., Scranton, Pennsylvania, 2nd. Edition, 1965, pp. 364-400.

17. Gomez, A. V., "Reentry Vehicle Injection Cooled Nosetip (U)," TRW Report No. 999900-6855-R3-00 (Secret, Group 3), January 1969.

18. Gomez, A. V., "Part I: R/V Nosetip Transpiration Cooling Theory and Application to the Development of TRW Transpiration Cooling Computer Programs," TRW Report No. 99900-6855-RO-01, February 1969.

19. Koh, J.C.Y., del Casal, E. P., Evans, R. W., and Deiriugin, V., "Fluid Flow and Heat Transfer in High Temperature Porous Matrices for Transpiration Cooling," Technical Report AFFDL-TR-66-70, Boeing Co., May 1966.

20. Koh, J.C.Y., and del Casal, E., "Heat and Mass Flow Through Porous Matrices for Transpiration Cooling," Proceedings of the 1965 Heat Transfer and Fluid Mechanics Institute, pp. 263-381.

21. Kelley, J. B., L'Ecuyer, M. R., "Transpiration Cooling - Its Theory and Application," Report No. TM-66-5, Jet Propulsion Center, Purdue University, June 1966.

22. Greenberg, D. B., and E. Weger, "An Investigation of the Viscous and Inertial Coefficients for the Flow of Gases Through Porous Sintered Metals with High Pressure Gradients," Chemical Engineering Science, March 1960.

23. Joint Army, Navy, Air Force Thermochemical Panel JANAF Thermochemical Tables, USAF Contract FO4611-67-C-0009, December 1964 (last revised 1966).

24. Dergazarian, E. T., et al., "JANAF Thermochemical Tables", Thermal Laboratory, The DOW Chemical Company, Midland, Michigan, December 1960 and supplements to date.

25. D'Amur, I. and Mason, E. A., "Properties of Gases at Very High Temperatures", The Physics of Fluids, Vol. 1, No. 5, Sept. - Oct. 1958, pp. 370-383.

26. Duff, R. E. and Bauer, S. H., "Equilibrium Composition of the C/H System at Elevated Temperatures", Journal Chem. Phys., Vol. 26, April 1962, p. 1754.

27. Hirschfelder, J. O., Curtiss, C. F., and Bird, R. B., Molecular Theory of Gases and Liquids, 2nd edition, J. Wiley and Sons, November 1965.

28. Svehla, R. A., "Estimated Viscosities and Thermal Conductivities of Gases at High Temperatures", NASA TR R-132, 1962.

29. Hochstim, A. R, "Equilibrium Compositions, Thermodynamic and Normal Shock Properties of Air with Additatives", Vol. 1, Zph-122, 1961, General Dynamics, Convair.

30. Wilke, C. R., "A Viscosity Equation for Gas Mixtures", Journal of Chemical Physics, Vol. 18, No. 4, April 1950, p. 517-519.

31. Mason, E. A., and Saxena, S., "Approximate Formula for the Thermal Conductivity of Gas Mixtures", The Physics of Fluids, Vol. 1, No. 5, September-October 1958, p. 361-369.

32. Johnston,C.G. and Gomez,A.V., "Radiative, Ablative, and Active Cooling Thermal Protection Studies For The Leading Edge of a Fixed-Straight Wing Space Shuttle, Part V: Transpiration Cooled Heat Shields Performance," TRW Report No. 17618-H076-R0-00, 31 December 1970.

END

DATE

FILMED

MAR 11

1972